Şeyda Tuğba GÜNDAY

M.S. Thesis In Chemistry

January 2007

SYNTHESIS AND PROTON CONDUCTIVITY OF MODEL POLYMER TRIAZOLE HYBRID ELECTROLYTES

by

Şeyda Tuğba GÜNDAY

January 2007

SYNTHESIS AND PROTON CONDUCTIVITY OF MODEL POLYMER-TRIAZOLE HYBRID ELECTROLYTES

by

Şeyda Tuğba GÜNDAY

A thesis submitted to

the Graduate Institute of Science and Engineering

of

Fatih University

in partial fulfillment of the requirements for the degree of

Master of Science

in

Chemistry

January 2007
Istanbul, Turkey

APPROVAL PAGE

I certify that this thesis satisfies all the requirements as a thesis for the degree of Master of Science.

Assist. Prof. Dr. Metin TÜLÜ

Head of Department

This is to certify that I have read this thesis and that in my opinion it is fully adequate, in scope and quality, as a thesis for the degree of Master of Science.

Assoc. Prof. Dr. Ayhan BOZKURT

Supervisor

Examining Committee Members

Assoc. Prof. Dr. Ayhan BOZKURT _____

Assoc. Prof. Dr. Ali ATA _____

Assist. Prof. Dr. Abdülhadi BAYKAL _____

It is approved that this thesis has been written in compliance with the formatting rules laid down by the Graduate Institute of Sciences and Engineering.

Assist. Prof. Dr. Nurullah ARSLAN

Director

January 2007

SYNTHESIS AND PROTON CONDUCTIVITY OF MODEL POLYMER TRIAZOLE HYBRID ELECTROLYTES

Şeyda Tuğba GÜNDAY

M. S. Thesis - Chemistry
January 2007

Supervisor: Assoc. Prof. Dr. Ayhan BOZKURT

ABSTRACT

Polymer electrolyte membrane fuel cells (PEMFC) have attracted remarkable interest due to conversion of chemical energy into electrical energy. In this context, the production of alternative membranes with high proton conductivity is becoming crucial. In this study, 1H-1,2,4-triazole (Tri) was used as a proton solvent in different polymer host matrices such as alginic acid AL, poly(vinylphosphonic acid), PVPA and poly(2-acrylamido-2-methyl-1-propane sulfonic acid), PAMPSA. $ALTri_x$, $PVPATri_x$ and $PAMPSATri_x$ electrolytes were investigated where x is the molar ratio of Tri to corresponding polymer repeat unit. The interaction between polymer and Tri was studied via FT-IR spectroscopy. Thermogravimetry analysis (TG) and differential scanning calorimetry (DSC) were employed to examine the thermal stability and homogeneity of the materials, respectively. The proton conductivity increases with the Tri content and $ALTri_{1.5}$ exhibited a maximum conductivity of ~ 10^{-4} S/cm at 100 ^{o}C. $PVPATri_{1.5}$ showed a maximum water-free proton conductivity of $2.3x10^{-3}$ S/cm at 120 ^{o}C and that of $PAMPSATri_2$ was $9.3x10^{-4}$ S/cm at 140 ^{o}C.

Keywords: Alginic acid, 1,2,4-Triazole, polymer electrolyte, anhydrous proton conductivity, poly(vinylphosphonic acid), poly(2-acrylamido-2-methyl-1-propane sulfonic acid).

MODEL POLİMER TRİAZOL ELEKTROLİTLERİN SENTEZİ VE PROTON İLETKENLİKLERİ

Şeyda Tuğba Günday

Yüksek Lisans Tezi - Kimya
Ocak 2007

Tez yöneticisi: Doç. Dr. Ayhan BOZKURT

ÖZ

Polimer elektrolit membran yakıt hücrelerine (PEMFC) olan ilgi kimyasal enerjiyi elektirik enerjisine dönüşümleri nedeniyle giderek artmaktadır. Bu bağlamda, yüksek proton iletken alternatif membranların geliştirilmesi oldukça önemlidir. Bu çalışmada, 1H–1,2,4-triazol (Tri), değişik matrislerde proton solvent olarak kullanılmıştır. Üzerinde çalışılan bu farklı matrisler alginik asit (AL), polivinilfosfonik asit (PVPA) ve poli-2-akrilamido-2-metil–1-propan sülfonik asit (PAMPSA) olarak seçilmiştir. $ALTri_x$, $PVPATri_x$ ve $PAMPSATri_x$ elektrolitleri incelenmiştir. Buradaki "x", polimer tekrar birimine karşılık gelen Tri'nin molar oranını ifade etmektedir. Polimer ve Tri arasındaki etkileşim FT-IR spektroskopi yardımıyla araştırılmıştır. Maddelerin termal sabitliklerini ve homojenliklerini incelemek için termal ağırlık analizi (TGA) ve diferansiyel taramalı kalorimetre (DSC) kullanılmıştır. Proton iletkenliği, Tri içeriğiyle artmaktadır ve $ALTri_{1,5}$, 100 ^oC sıcaklıkta 10^{-4} S/cm gibi maksimum bir iletkenlik göstermiştir. $PVPATri_{1.5,}$ 120 ^oC sıcaklıkta $2,3x10^{-3}$ S/cm lik maksimum nemsiz proton iletkenliği gösterirken, nemsiz $PAMPSATri_2$'nin 140 ^oC deki maksimum proton iletkenliği $9,3x10^{-4}$ S/cm olarak ölçülmüştür.

Anahtar Kelimeler: Alginik asit, 1,2,4-Triazol, polimer elektrolit, nemsiz proton iletkenlik, poli(vinilfosfonik asit), poli(2-akrilamido-2-metil–1-propan sülfonik asit).

DEDICATION

To my dear, precious, and esteemed family

ACKNOWLEDGMENT

First of all, I would like to thank my thesis supervisor Assoc. Prof. Dr. Ayhan BOZKURT. His motivation and power kept me doing all the work. His academic activities will be references in my future studies.

This work is supported by TÜBİTAK under the contract number 104M220.

I would like to thank Dr. Wolfgang MEYER for providing me remarkable opportunities in the Max-Plank Institut für Polymerforschung-Mainz where part of the characterizations were carried out.

I would like to thank Research Assistant İsmail Anıl for his kind help.

I would like to thank friends of my department for time support and patience.

Finally, I would like to thank my parents for their love, patience and encouragement.

TABLE OF CONTENTS

LIST OF TABLES

TABLE

LIST OF FIGURES

FIGURE

LIST OF SYMBOLS AND ABBREVATIONS

SYMBOLS/ABBREVATIONS

SPE	Solid Polymer Electrolytes
PVPA	Poly(vinylphosphonic acid)
PAMPSA	Poly(2-acrylamido-2-methyl -1-propanesulfonic acid)
PEM	Proton Exchange Membrane
PEMFC	Proton Exchange Membrane Fuel Cell
PTFE	Poly(tetraflouroethylene)
PBI	Polybenzimidazole
PEO	Poly(ethylene oxide)
PEI	Poly(ethyleneimine)
PAAM	Poly(acrylamide)
P-4VI	Poly(4-vinyl-imidazole)
Py	Pyrazole
MeIm	1-methylimidazole.
PAA	Polyacrylic Acid
MDP	Mono-dodecylphosphate
MP	Methanediphosphonic Acid
AFC	Alkaline Fuel Cell
PAFC	Phosphoric Acid Fuel Cell
MCFC	Molten Carbonate Fuel Cell
ITSOFC	Intermediate Temperature Solid Oxide Fuel Cell
TSOFC	Tubular Solid Oxide Fuel Cell
ECD	Electrochromic Device
EC	Electrochemical Cell
VTF	Vogel-Tammann-Fulcher

CHAPTER 1

INTRODUCTION

The synthesis of novel proton conducting polymer electrolytes with variety of properties has been the focus of polymer research for many years due to possibility of their application in various electrochemical devices, e.g., fuel cells and electrochromic devices.

For decades, no other type of material was found to be competitive. However, these membranes remain expensive and have several limiting factors such as low conductivity at low relative humidity (Sumner et al., 1998), highly methanol crossover (Schuster et al., 2003) and a low T_g (glass transition temperature) (Samms et al., 1996) which restricts its application to below 100 ^{o}C. In addition to these factors, which decrease the total efficiency of the system, the high price, as well as difficult recycling or disposal of the perfluorinated materials, has slowed wide-spread and economical application.

Accordingly, a variety of alternative approaches using materials that are cheaper and/or more suitable for higher temperatures have been explored, among which are non-fluorinated ionomers and composite membranes. Solid polymer electrolytes (SPE) that have high proton conductivity at higher temperatures are important for the conversion of chemical energy into electrical energy by means of fuel cells (Smitha et al., 2005, Schuster and Meyer, 2003). SPEs are also significant for solid state electrochromic devices only if the materials are compatible with electrode devices, transparent and in the dry state (Schuster and Meyer, 2003). During last few decades, several kinds of proton conducting SPE have been developed. Polymer–acid complexes were the first approach in which basic or neutral polymers were blended with strong acids and they have already been shown to possess high proton conductivity in the anhydrous state

(Schuster and Meyer, 2003, Bozkurt and Meyer, 2001). Alternative proton conducting membranes have also been developed through blending of heterocyclic compounds such as imidazole and benzimidazole by acidic host polymers (Yamada and Honma, 2005, Erdemi et al., 2004). In these systems, proton transport occurs between hydrogen-bonded neighboring heterocyclic units through structure diffusion (Münch et al, 2001).

1H-1,2,4-Triazole (Tri) is another promising heterocycle whose melting point is 120 °C and boiling point is 260 °C. Tri is a crystalline solid at room temperature and different from imidazole, it contains three nitrogen atoms in the ring. Although the proton conductivity of pure 1H-1,2,4-triazole was reported to be near $1x10^{-4}$ S/cm at 115 °C and $1.2x10^{-3}$ S/cm at the melting point (Li et al., 2005), the mechanical property appears to be inadequate for fuel cell application. The use of Tri as a blend component in an acidic polyelectrolyte can be useful for the development of high temperature resistive free standing films. Since polymer electrolyte membranes consisting of acidic polymer host and Tri may allow long range proton transport via structure diffusion. Previously, the reactions paths of different proton transfer reactions in 1,2,3-Triazole have been investigated by computational methods and deduced that Tri forms clusters that favors intermolecular proton transfer reactions (Rauhut, 2003).

CHAPTER 2

ANHYDROUS PROTON-CONDUCTING POLYMERS

Since their development in the 1960s, perfluorinated ionomers have emerged as standard materials for low-temperature fuel cell applications because of their high proton conductivity and their excellent chemical and thermal stability. For decades, no other type of material was found to be competitive, despite intense research and a number of severe limitations impeding an economical and wide-spread application of proton exchange membrane (PEM) fuel cells. Without doubt, the most extensive limitations arise from the fact that these materials are proton-conducting only when hydrated, which results in a maximum operating temperature of ~ 100 °C that in turn limits activity and CO tolerance of the electro catalyst. Other drawbacks of this type of membrane are the need of permanent humidification (i.e., of additional peripheral devices), high methanol crossover, and limited mechanical stability (Schuster and Meyer, 2003).

In addition to these factors, which decrease the total efficiency of the system, the high price, as well as difficult recycling or disposal of the perfluorinated materials, has slowed wide-spread and economical application. Accordingly, a variety of alternative approaches using materials that are cheaper and/or more suitable for higher temperatures have been explored, among which are non-fluorinated ionomers and composite membranes (discussed elsewhere in this chapter). The polymeric materials in which proton conduction does not depend on the presence of an aqueous phase. In general, there are two fundamental approaches toward such membranes. The first one is simply based on the substitution of the water with another suitable proton solvent that is capable of conducting protons in a similar way at higher temperatures. Phosphoric acid has attracted most attention in this context, but aromatic heterocycles are also promising. A second approach points toward fully polymeric

systems that exhibit proton conductivity as an intrinsic property. In principle, these materials consist of an acid-doped proton acceptor (or vice versa) that forms mobile protonic defects (excess protons or proton vacancies, respectively). However, the development of a highly conductive all-solid polymer is far from trivial and requires careful tuning of the polymer's properties (Schuster and Meyer, 2003).

2.1 PHOSPHORIC ACID-BASED MEMBRANES

The property of phosphoric acid to interact via hydrogen bonds facilitates the preparation of blends with a large variety of polymers. In the case of basic polymers, proton transfer from phosphoric acid to the polymer helps for a wide miscibility of these complexes. However, the miscibility limits of phosphoric acid-polymer blends are often unknown, and some of the systems reported in the literature in reality may be inhomogeneous.

Phosphoric acid is a weak acid (pKa = 2.16) (Lide, 1995) that melts at 42 °C in the pure state and acts as an oxidant at elevated temperatures. With basic polymers, phosphoric acid undergoes hydrogen bond interactions or proton transfer reactions. In regard to its conductivity, phosphoric acid differs from water and many other solvents in two ways. First, conductivity is remarkably high in the pure state (Chin and Chang, 1989). Second, when strong electrolytes (e.g., H_2SO_4) are added, conductivity decreases rather than being improved (Munson and Lazarus, 1967). The first feature is due to the generation of charge carriers by self-dissociation ($5H_3PO_4 = 2H_4PO_4^+ + H_2PO_4^- + H_3O^+ + H_2P_2O_7^{2-}$, where H_3PO_4 = 16.8 M, $H_4PO_4^+$ = 0.89 M, $H_2PO_4^-$ = 0.43 M, H_3O^+ = $H_2P_2O_7^{2-}$ = 0.46 M at 311 K) and the fact that proton migration almost entirely results from structure diffusion (Dippel and Kreuer, 1993). The second feature is also closely related to the transport mechanism. The electrical field of extrinsic charge carriers causes a bias on hydrogen bonds and thus suppresses fluctuations within the dynamical hydrogen bond network (Kreuer, 1996, Kreuer, 2000). Addition of water, however, increases conductivity, which passes through a temperature-dependent maximum at compositions of 45 to 60% of H_3PO_4 (Chin and Chang, 1989).

2.1.1 P-4VI/H_3PO_4

Poly(4-vinyl-imidazole), P-4VI, and phosphoric acid blends are reported (Bozkurt and Meyer, 2001).The number of moles of phosphoric acid per polymer repeat unit, x, was varied from $0 \leq x \leq 2$ .These blends can be cast into homogeneous films. These blends are chemically stable up to about 150 °C. The softening temperature of the blends decrease from 77 °C for x = 1 to -8 °C for x = 2. Bozkurt and Meyer, 2001 was found the DC conductivity increases with x and reaches ~10^{-4} S/cm for x = 2 at ambient temperature.

2.1.2 PEO/H_3PO_4

PEO/H_3PO_4 complexes (x = 0.42 – 0.66) were described in 1988 by Donoso et al., who found conductivities of 2.5 x10^{-4} S/cm at 50 °C (x = 0.42) governed by segmental motion of the polymer chains. Przyluski et al. reinvestigated these blends covering a wider range of compositions ($0.06 \leq x \leq 2.8$) by means of differential scanning calorimetry (DSC), IR, Vogel-Tamman-Fulcher (VTF), and impedance spectroscopy and found VTF behavior for small x and Arrhenius behavior for larger x. The molar amount of acid per mol of polymer repeating units is described by x.

2.1.3 PEI/H_3PO_4

PEI/H_3PO_4 blends ($x \leq 0.5$) were introduced by Daniel et al., 1988, who found conductivities of 1 to 3x10^{-3} S/cm at 100 °C. At x = 0.35, a precipitate was formed from the aqueous solution, which redissolved upon further addition of H_3PO_4 (x = 0.58). Schoolman et al. characterized blends of higher acid contents ($x \leq 2$) that were applied as electrolytes for electrochromic devices. Whereas these researchers (Daniel et al., 1988, Schooleman et al., 1992) used branched commercial PEI. Tanaka et al., 1995, compared branched and linear PEI and found somewhat higher conductivities for the latter; however, compared with the results from Daniel et al., conductivities of the branched materials were about two orders of magnitude lower, which were attributed to the different preparation and purification procedures.

Composition-dependent conductivities of branched and linear PEI blends (Daniel et al., 1988, Tanaka et al., 1995) exhibited a local maximum at $x \approx 0.2$ and dropped to a minimum at $x \approx 0.4$, where the formation of PEI-H^+ 1/2 HPO_4^{-2} was completed (the maximum degree of protonation of PEI is ~ 80%) (Bloys and Staverman, 1974). This behavior is in accordance with a maximum Tg of the blend (Daniel et al., 1988, Lassegues et al., 1989) and the precipitation from aqueous solution (Daniel et al., 1988) at $x \approx 0.35$. At higher acid levels, conductivity increased again and achieved values of 1.4×10^{-3} S/cm (^{l}PEI, $x = 2.05$; 100 ^{o}C) (Tanaka et al., 2000).

Properties of the hygroscopic, deliquescent linear PEI blends could be improved by crosslinking, which moderately influences conductivity at high x, but nearly reverses its dependence on composition at low x (Tanaka et al., 2000).

2.1.4 PAAM/H_3PO_4

PAAM/H_3PO_4 blends showed relatively high conductivities (4×10^{-3} S/cm, 20^{o}C, x = 2). However, condensation of the amide groups was observed at 100 ^{o}C in dry air (Rodriguez et al., 1993).

2.1.5 PBI/H_3PO_4

In 1995, a blend of poly(benzimidazole) and phosphoric acid was considered for hydrogen fuel cell and direct methanol fuel cell (DMFC) applications for the first time (Wainright et al.,1995). PBI is an amorphous (Singleton et al., 1967, Buckeley et al., 1988), basic polymer (benzimidazole: pKa = 5.5) (Lide, 1995) of extraordinary thermal stability and a glass transition temperature of about 430^{o}C (Singleton et al., 1967, Gilham, 1972). Qingfeng et al. found that the conductivity of PBI–H_3PO_4 complexes was insensitive to humidity, but strongly dependent on the acid content, reaching values of 0.13 S/cm at 160 ^{o}C and high acid-doping levels (Qingfeng et al., 2001). It was also shown that the water drag due to proton transport was almost zero in these PEMs. Wasmus et al. used solid-state NMR characterization of H_3PO_4 doped PBI to show that the phosphoric acid sorbed by the PBI membrane was relatively immobile as compared to free phosphoric acid, and revealed that there was an interaction between imidazole

groups of PBI and phosphoric acid (Wasmus et al., 1995). Glipa et al. confirmed proton transfer from H_3PO_4 to the imino groups of PBI and the presence of undissociated H_3PO_4 at high doping levels with IR spectroscopy (Glipa et al., 1999). Li et al. measured conductivity as a function of temperature and a wide range of acid doping levels (x = 3.0 ~ 16.0, where x is acid molecule per polymer repeat unit) at R.H. between 80% ~ 85%. They obtained a conductivity of 4.6×10^{-2} S/cm at 165 ^{o}C. They suggested a useful H_3PO_4 doping level between 3.5 ~ 7.5, considering both conductivity and mechanical strength (Li et al., 2001). Kawahara et al. prepared H_3PO_4 doped PBI membranes by immersing the PBI membranes into a mixed solution of acid and methanol. The highest doping level observed was 2.9 mol H_3PO_4/repeat unit. Based on FTIR data, they concluded that H_3PO_4 did not protonate the imidazole groups of PBI but interacted by hydrogen bonding between the OH and N groups. The presence of HPO_4^{2-} and $H_2PO_4^{-}$ anions, based on FTIR, implied that the proton conduction occurred according to the Grotthuss mechanism. The conductivity of the anhydrous PBIX2.9H_3PO_4 complex reached 10^{-4} S/cm at 160 ^{o}C. Fontanella et al. measured the isobaric conductivity data of PBIX6.H_3PO_4 membrane at temperatures of 25, 50, and 75 ^{o}C. Based on the activation volume values (4~7 cm^3/mol), they proposed that proton transport in the acid doped PBI was mediated by segmental motions of the polymer (Fontanella et al., 1998). Pu, et al. proposed that proton transport in phosphoric acid blended PBI was the consequences of the two contributions: one was based on rapid proton exchange (hopping) via hydrogen bonds between solvent molecules, which could be the phosphate, N-heterocycles of PBI and water molecules; and the other was based on the self-diffusion of phosphate moieties and water molecules (vehicle mechanism). They studied the temperature and pressure dependence of the conductivity of PBIxH_3PO_4 membranes (x = 1.8~3.8) (Pu et al., 2002).

Compared with the established Nafion^{TM} membranes, PBI is superior in several critical properties. PBI was reported (Savadogo and Varela, 2001) to be about 100 times cheaper than Nafion at present PBI is exclusively produced by Celanese Corporation, who offer only complete membrane electrode assemblies (MEA) for operating temperatures of up to 200^{o}C. Singleton et al. claim a considerably higher mechanical strength of doped PBI than that of Nafion (Singleton et al., 1967, Wainright et al., 1995).

2.2 POLYMER/HETEROCYCLE HYBRID MATERIALS

2.2.1 Polymer Composite Materials

2.2.1.1 PVPA-Heterocycle Composite Materials

Yamada and Honma have prepared the acid–base composite materials by mixing of a strong phosphonic acid polymer poly(vinylphosphonicacid) (PVPA) with the high proton exchange capacity and an organic base heterocycle, such as imidazole (Im), pyrazole (Py), and 1-methylimidazole (MeIm) (Figure 2.1). This PVPA-heterocycle composite material exhibited a large proton conductivity of $7x10^{-3}$ S/cm at 150 °C under anhydrous condition. Additionally, the thermal stability of composite material was found to increase with the mixing ratio of the heterocycle.

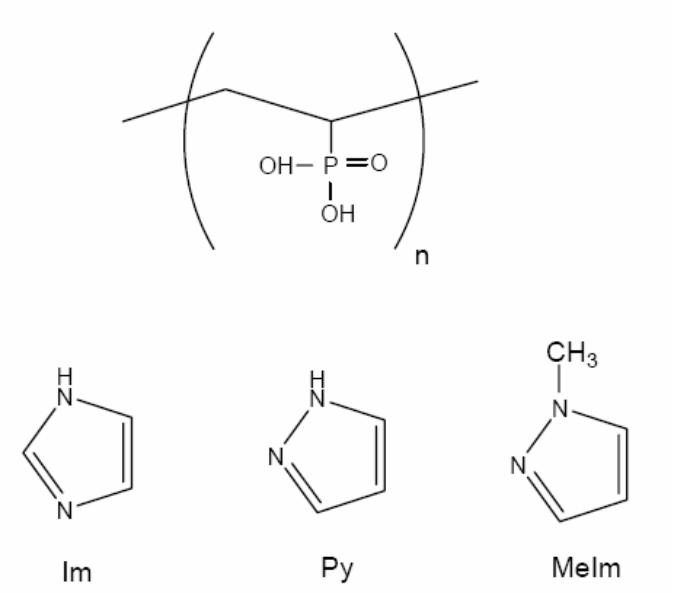

Figure 2.1 Molecular structures of poly(vinylphosphonicacid) (PVPA) , imidazole (Im), pyrazole (Py), and 1-methylimidazole (MeIm).

Anhydrous proton conductivity of PVPA-heterocycle composite materials showed differences of approximately one order of magnitude, depending on the molecular structure of basic heterocycles. These different conductivities of composite materials are due to the pKa value of heterocyclic molecules. The pKa values of heterocycle

molecules (Acheson, 1976) and the maximum proton conductivity at 150 °C under anhydrous condition are listed in Table 2.1. The basicity of heterocycle molecules of Im is larger than that of Py (see the pKa1 value in Table 2.1). Clearly, the conductivity of PVPA-Im composite material is larger than PVPA-Py composite material. These results suggest that pyrazole molecule with the low basicity do not act as a proton donor and acceptor in composite material since the free proton from the PVPA molecule could not strongly interacts with non-protonated –N= group of pyrazole ring. In contrast, the pKa1 value of MeIm molecules is as same as that of Im molecules. However, the conductivity of PVPV-MeIm composite material is lower than that of PVPA-Im. This phenomenon is due to the molecular structure of imidazole. The Im molecules have been reported the construction of molecular cluster, consisting of approximately 20 molecules (Acheson, 1976), through the intermolecular hydrogen bonding.

As a result, PVPA-Im composite material might possess fast proton transfer of inter-heterocycle molecules in the composite material. However, MeIm molecules do not construct the molecular cluster with the intermolecular interaction in membrane and cannot provide fast proton transfer kinetics in inter heterocycle molecules. Based on the basicity and clustering mechanism, PVPA-Im composite material are supposed to possess the highest proton conductivity of $7x10^{-3}$ S/cm at 150 °C under anhydrous condition in many different types of PVPA-heterocycle composite materials. These results suggest that the basicity and molecular structure of heterocycle in acid-base composite material are important factors to obtain the anhydrous proton conductivity at the intermediate temperature condition (Yamada and Honma, 2005).

Table 2.1 Maximum proton conductivities of PVPA-heterocycle composite material and acid dissociation constant (pKa values of various heterocycle molecules). a is maximum proton conductivity 150 ^{o}C under anhydrous condition and b is reference (Acheson, 1976)

PVPA-heterocycle	Maximum conductivity [a] (S/cm)	Pka value of heterocycle [b] Pka1	Pka2
PVPA-Im	7×10^{-3}	7.2	14.5
PVPA-Py	8×10^{-4}	2.5	14
PVPA-MeIm	1×10^{-3}	7.4	

In 2003, anhydrous proton conducting polymer electrolytes have been prepared by entrapping imidazol (Im) in polyacrylic acid (PAA) with various stoichiometric ratios, x, to form PAAxIm (x is the number of moles of Im per polymer repeat unit) (Figure 2.2) (Meyer et al., 2003). Polymer electrolytes, PAAxIm (with x = 0.5 and 1) can be cast into transparent, homogeneous films which are thermally stable up to 200 °C. From FT-IR spectra it is evident that hydrogen bonds exist between protonated and unprotonated Im units. With increasing Im content the glass transition temperature decreases while their conductivity increase, reaching 10^{-3} S/cm at 120 °C.

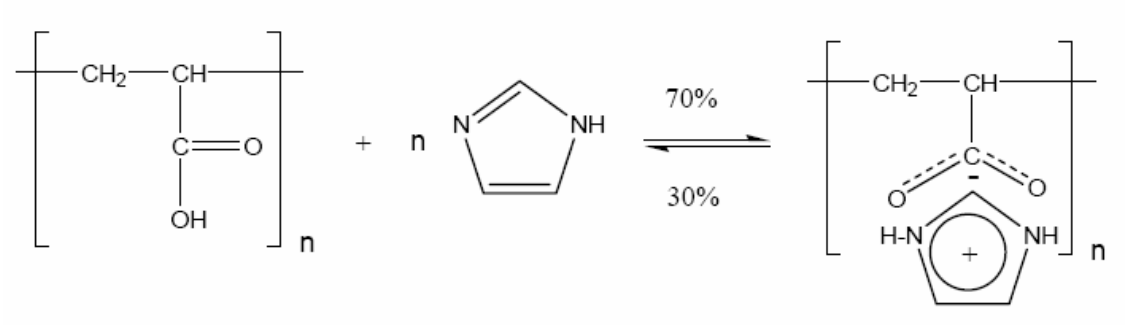

Figure 2.2 Illustration of the protonation of imidazol upon blending with PAA (Meyer et al., 2003).

It was previously mentioned that the membrane materials based on carboxylic acid groups shows no significant proton conductivity even at higher level of hydration. Because –COOH groups are less sensitive to hydrolysis and higher pKa values (Kreuer, 1996).

The intercalation of imidazol with different doping ratio, x into PAA as Brønstedt acid increased the conductivity PAAxIm membranes. The reason may be imidazol, like water, acts as proton donor and acceptor in the proton conduction process. In this sense it behaves amphoteric but with respect to other compounds they are more basic than water (Kreuer, 1998). FT-IR of PAAxIm confirmed that imidazol is partially protonated from “free” nitrogen side. A Grotthuss type diffusion mechanism may explain the proton diffusion process within protonated and unprotonated heterocycles. Because the

protonic defect may cause local disorder by forming (. . . Him-(HimH+)-imH. . .) configuration as discussed in the literature (Münch et al., 2001). The use of imidazol in a suitable acidic host polymer to increase the concentration of defect protons may also technological interest. Further systems like PAMPSA-imidazole are under investigation and will be communicated soon.

2.2.2 Other Composite Materials

2.2.2.1 Benzimidazole/Monododecyl Phosphate Molecular Hybrids

It had been reported that a glass-filter supported monododecyl phosphate/benzimidazole mixed material shows a high proton conductivity of $1x10^{-3}$ S/cm at T = 150 ^{o}C underwater-free conditions along with a high thermal stability (Yamada and Honma, 2003). Even other acid–base hybrid materials resulted in the same anhydrous conductor at elevated temperatures (Yamada and Honma, 2004, Yamada and Honma, 2004). Kim and Honma investigated the effects of monododecyl phosphate (MDP) doping to benzimidazole (BnIm) by IR, TG, XRD, proton conductivities. The XRD results showed new phases different from the crystal structures of MDP and BnIm (Figure 2.3), and the doping of MDP displayed the peaks of BnIm due to the extinction rule of reflection. The hybrids showed a high proton conductivity of $1x10^{-2}$ S/cm above 100 ^{o}C under a non-humidified (anhydrous) condition (Kim and Honma, 2005).

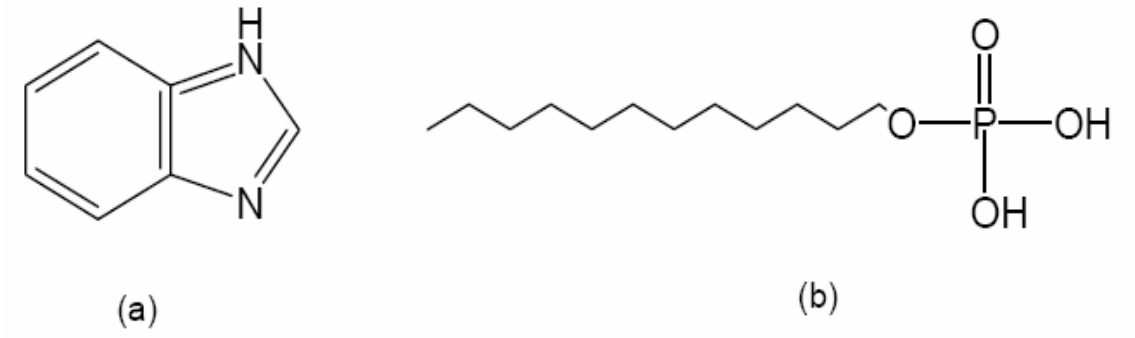

Figure 2.3 Molecular structures of (a) benzimidazole and (b) monododecyl phosphate.

2.2.2.2 Alginic Acid-Imidazole Composite Material

Other anhydrous proton conductor consisting of alginic acid (AL), one of the acidic biopolymers, and imidazole (Im) molecules, one of the basic heterocyclic molecules was reported by Yamada et al. in 2004. This AL-Im ($r \geq 20$) composite material indicated the high proton conductivity of $2x10^{-3}$ S/cm at 130 °C. On the other hand, the activation energy, such as 1.2-1.6 eV, at $r \leq 1$ is extremely larger than that of other reported materials. This high activation energy is due to the long distance between the hopping sites. Additionally, the proton hopping distance of pure AL or small mixed material ($r \leq 0,5$) was too long to hop to neighboring site, as a result, these materials could not show any measurable proton conductivity ($< 10^{-8}$ S/cm) (Yamada and Honma, 2004).

The bimolecular composite material, such as chitin phosphate-hetrocyclic molecules composite materials as an anhydrous proton conducting membrane was reported by (Yamada and Honma 2004). In these cases, the composite materials showed the high proton conductivity of $\geq 10^{-3}$ S/cm at 150 °C under anhydrous condition. Additionally, these materials had a high thermal stability. However, AL-Im composite materials did not indicate the satisfactory conductivity and thermal stability in comparison with the reported materials (Yamada et al., 2003, Yamada et al., 2004). One of the reasons might be the effect of pKa value (pKa = 3.1) of –COOH group in AL (Jang et al., 1996). Phosphonic acid is stronger than carboxylic acid. The phosphonic acid group and basic group forms a strong acid-base complex in the composite membrane, as a result the free proton from phosphonic acid strongly interacts with non-protonated –n═ (Yamada et al., 2003, Yamada et al., 2004). However a weak acid, such as –COOH group in AL, cannot form the strong acid-base in composite membrane and not provide enough mobile-protons to Im molecules, so that AL-Im composite showed the lower anhydrous proton conductivity than the phosphonic acid composite materials (Yamada and Honma, 2004).

2.2.2.3 Adipic Acid/Benzimidazole Hybrid Electrolytes

Bozkurt et al. investigated several blends of a diacid, adipic acid (AA) (Figure 2.4) and heterocyclic base, benzimidazole (BnIm). Adipic acid has very low proton conductivity (~ 10^{-11} S/cm) in crystalline form. The conductivity of the blends increased with BnIm and reached a maximum conductivity of $4x10^{-3}$ S/cm at 130 ^{o}C (Karadedeli et al., 2005).

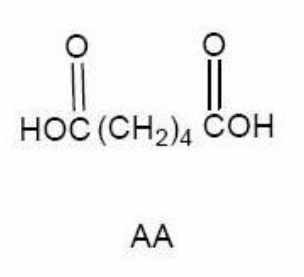

Figure 2.4 Moleculer structure of AA

From DSC results, it can be concluded that such conductivity increase within this temperature regime may be the effect of first-order transition (melting) onto the ionic conductivity of the samples. At higher temperatures, (T > 373 K) the conductivities of these samples are very close to each other irrespective of their BnIm content. High BnIm doping levels ($BnIm_2AA$) result in higher conductivity even at lower temperatures. This behavior may reflect the ambivalent role of hydrogen bonding as already observed for the proton mobility in heterocyclic systems (Kreuer et al., 1998). Previously the proton conductivity in anhydrous heterocycles, i.e. imidazole and pyrazole, and their mixtures with H_2SO_4 and H_3PO_4 were investigated (Kreuer et al., 1998, Schuster et al., 2003).

The protonic defects are created by protonation of heterocycles which act as solvent for protons and it is the dynamics of these solvent molecules which lead to the mobility of the protonic defects, i.e. intermolecular proton transfer and structural reorganization by hydrogen bond breaking and forming processes (structure diffusion). The IR spectra of the BnImxAA indicate the partial protonation of benzimidazole which

occurs from the free N side forming benzimidazolium ion. Therefore, at higher temperatures, protons can be rapidly transferred to neighbor molecule with small activation energy. Similar behavior was observed in PAA-imidazole and mono-dodecylphosphate (MDP)-benzimidazole mixed materials (Bozkurt et al., 2003, Yamada et al., 2003). The BnImxAA blends showed a maximum conductivity of $4x10^{-3}$ S/cm at 130 °C in anhydrous state. The materials which comprise $–CO_2H$ acidic functional groups as part of their constitutional unit have not been preferred as proton conductors since these units are less sensitive to hydrolysis, have higher pKA values and hence yield low conductivity. This work was demonstrated that anhydrous, high proton conductive organic electrolytes can also be obtained when $–CO_2H$ containing materials are doped with benzimidazole (Karadedeli et al., 2005).

2.2.2.4 Anhydrous Proton Conductive Membrane Consisting of Chitosan

Other anhydrous proton conducting membrane using a composite of chitosan, one of the basic biopolymers with an amino group, and methanediphosphonic acid (MP), which possesses a large proton Exchange capacity was prepared by Honma and Yamada, in 2005 (Figure 2.5). This chitosan–MP composite material showed the high proton conductivity of 5×10^{-3} S/cm at 150 °C under anhydrous (water-free) conditions. The proton conducting mechanism of the chitosan–MP composite material was due to proton transfer to the proton defect site without the assistance of diffusible vehicle molecules. The utilization of a biopolymer, such as chitosan, for PEMFC technologies is novel and challenging where biological products are usually considered as waste, non-hazardous, and environmentally benign. Especially, the low production cost of the biopolymer is an attractive feature. Anhydrous proton conducting biopolymer composite membranes may have potential not only for PEMFCs operated under anhydrous conditions, but also for bio-electrochemical devices including an implantable battery, bio-sensors. Additionally, the thermal stability of this composite material was found to increase with the mixing ratio of the MP molecule (Yamada and Honma, 2005).

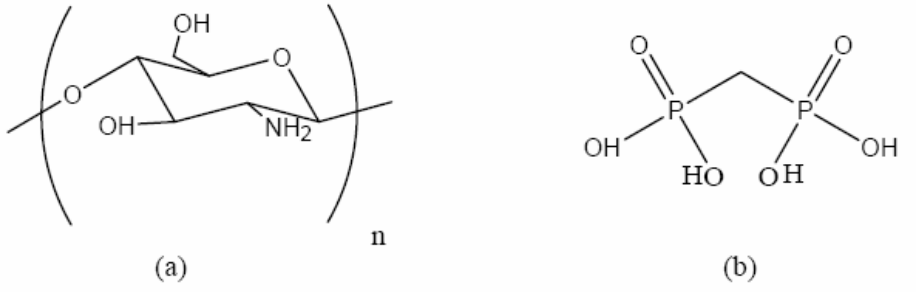

Figure 2.5 Molecular structures of chitosan (a) and methanediphosphonic acid (b) (MP).

CHAPTER 3

HYDRATED SULFONIC ACID MEMBRANES

The proton exchange membrane fuel cell (PEMFC) has recently been shown to be the most promising of all the fuel cell types for applications such as automobiles, stationary power and power for small electronics such as laptop computers and cell phones (Korgesch et al., 1996). A solid polymeric membrane containing ionic groups is responsible for the proton transport from the anode to the cathode. Polymer electrolyte fuel cells were the first type of fuel cell demonstrated in the space flight program. Originally, the proton exchange membrane (or alternatively polymer electrolyte membrane) was a sulfonated poly(styrene divinylbenzene) copolymer. These membranes showed very poor lifetimes due to oxidative degradation of the polymer backbone (Hickner, 2003).

In 1968 DuPont commercialized a proton exchange membrane based on poly (perfluorosulfonic acid) under the trade name Nafion (Grot, 1968). The highly fluorinated structure shown in Figure 3.1 displays a much greater resistance to degradation in a fuel cell environment and thus increasingly longer fuel cell lifetimes.

Since then, other companies, such as Asahi in Japan and briefly Dow in the U.S, have investigated membranes based on poly (perflurosulfonic acid) structures, but Dow has exited the business and Asahi remains a small player. Nafion has remained the industry standard proton exchange membrane and almost all current PEM fuel cell research from a device standpoint focuses on this type of electrolyte. Major applications for Nafion also include chlorine synthesis via electrolysis (chlorine-alkali processes) (Berzins, 1977).

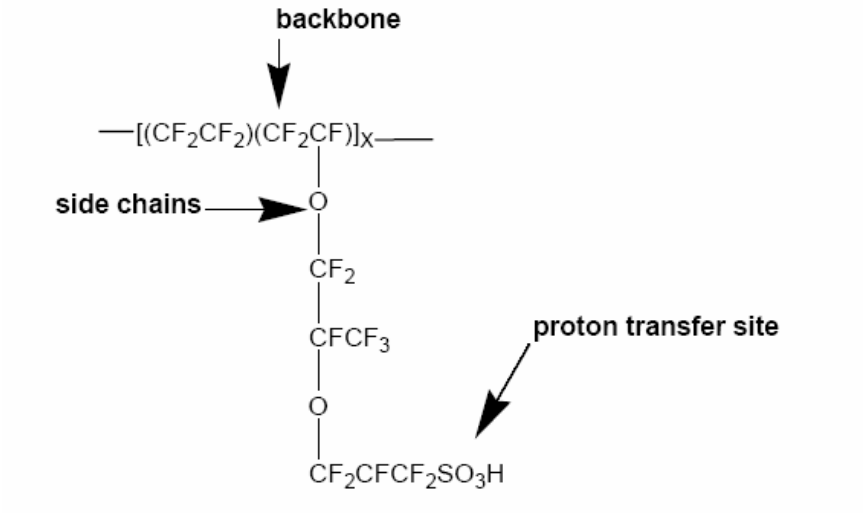

Figure 3.1 Molecular structure of Nafion

Nafion membranes are composed of carbon-fluorine backbone chains with perfluoro side chains containing sulfonic groups (Doyle et al., 2003). The Teflon-like molecular backbone gives these materials excellent long-term stability in both oxidative and reductive environments. A lifetime of over 60,000 hours has been achieved with commercial Nafion® membranes (Steck, 1995). These membranes exhibit a protonic conductivity as high as 0.10 S/cm under fully hydrated conditions. For a typical membrane thickness of, say, 175 μm (Nafion 117), this conductivity corresponds to a real resistance of around 0.2 Ωcm^2, i.e. a voltage loss of about 150 mV at a practical current density. The structure model of nafion membrane which comprises ionic hydrophilic clusters, an amorphous hydrophobic region is suggested previously (Figure 3.2) (Kreuer et al., 1993). The transport properties of perfluorosulfonic membranes largely influenced by the water content of the membrane, particularly when the membrane in the acidic form. The hydrophilic cluster swells with the water content. In the dry state Nafion membrane behaves like an insulator but, when hydrated the membrane becomes conductive (Yeo et al., 1983, Pourcelly et al., 1990). Proton conductivity reaches maximum over a temperature range 55-70 ^oC, even tough water content is minimum. Out with these temperature ranges, the conductivity decreases resulting from deionization of the sulfonic acid groups and perhaps a change of the hopping distance between cluster zones (Rieke and Vanderborgh, 1987).

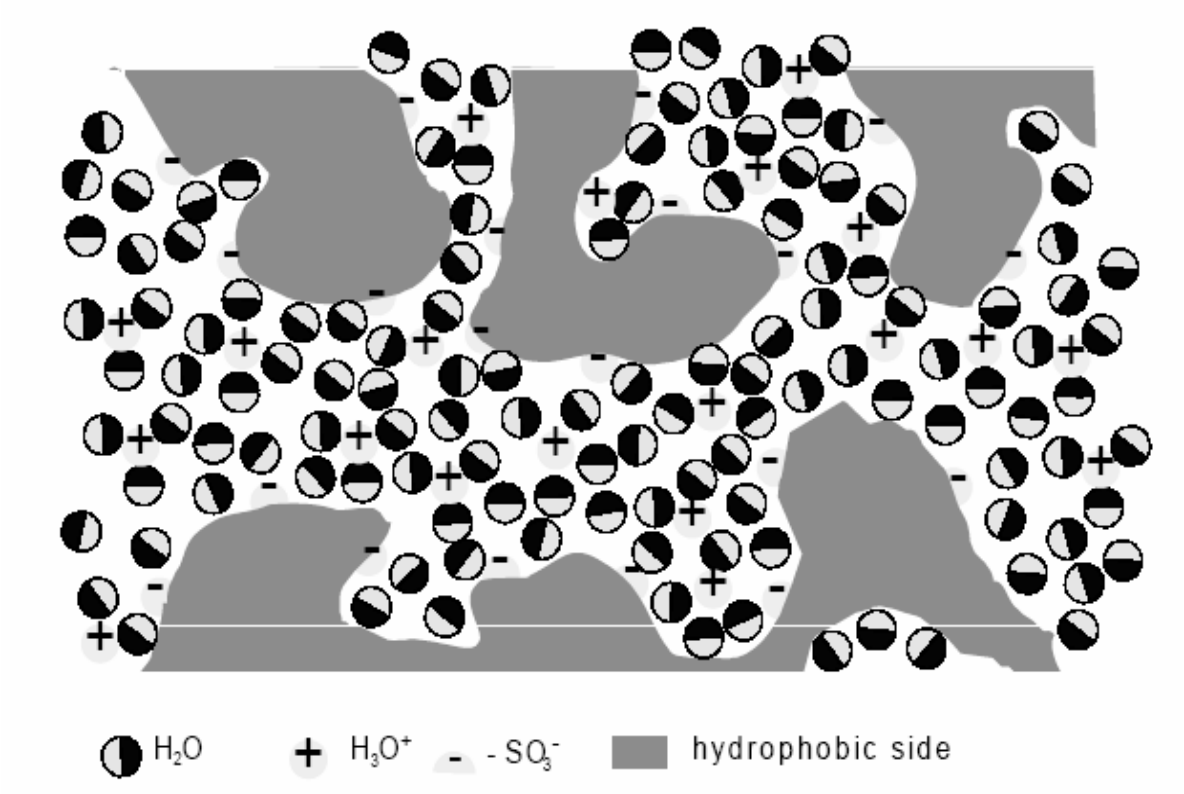

Figure 3.2 Structure model for Nafion perfluorosulfonic membrane (Kruer, 2001)

Ionomer-based membranes intended for high-temperature PEMFCs should preferably retain a high conductivity at low levels of humidification. Thus, there is a need to improve water retention at high temperatures and to improve performance at low water contents, while simultaneously giving special attention to chemical as well as morphological stability to resist excessive water swelling. The membrane morphology is important for the performance, and is linked to the nature of the ionomer and the membrane formation process in a quite complex manner. It typically depends strongly on the water content, and on the concentration and distribution of the acidic moieties (Kreuer, 2001, Ding, 2002, Tang, 2001). For example, Kreuer has shown that hydrated membranes based on sulfonated polyetherketone have a less pronounced separation into hydrophilic hydrophobic domains, as well as a larger distance between the acidic moieties, as compared to the Nafion membrane (Kreuer, 2001, Jannasch, 2003).

Perfluorinated PEMs have been developed by modification of the acid group (Hogarth and Glipa, 2001, Kotov et al., 1997). Thus, DesMarteau replaced the sulfonic acid group ($-SO_3H$) in Nafion with a sulfonyl imide group ($-SO_2NHSO_2CF_3$), which results in an increase in the water uptake while Kotov et al. developed membranes with a phosphonic acid group that has the potential for higher thermal stability (DesMarteau, 1995, Savett, 2002, and Kotov et al., 1997). Other perfluorinated PEMs include Gore-select which uses a PTFE matrix embedded in the perfluorinated PEM to provide mechanical strength, thus allowing membrane thickness to be reduced to below 20 mm. These membranes possess conductivity up to 0.01-0.1 S/cm depending on RH (Liu et al., 2001).

Partially fluorinated PEMs such as the sulfonated trifluorostyrene membranes have also been developed (Hogdon, 1968). Ballard Power Systems has developed BAM3G, a family of PEMs with equivalent weights 375 to 920, by incorporating a,b,b-trifluorostyrene monomer, and a series of substituted a,b,b-trifluorostyrene comonomers. These membranes are less expensive than Nafion and have demonstrated good stability (>15,000 h) (Steck and Stone, 1997).

The majority of the new ionomers developed currently are based on different arylene main-chain polymers, which are characterized by excellent thermal, chemical, and mechanical properties. Some of these ionomers are shown in Figure 3.3. Several research groups are working with different sulfonated polymers containing diarylsulfone units (Wang et al., 2002, Poppe et al., 2002, and Jönissen et al., 2002). For example, Wang et al. have prepared high molecular weight polysulfones containing randomly distributed disulfonated diarylsulfone units.

Analysis of the membrane morphology by atomic force microscopy revealed hydrophilic phase domains that increased in size, from10 to 25 nm, with increasing degree of sulfonation. The membranes were stable up to 220 °C in air, and highly sulfonated ones showed conductivities of 0.17 S/cm 30 °C in water (Wang et al., 2002).

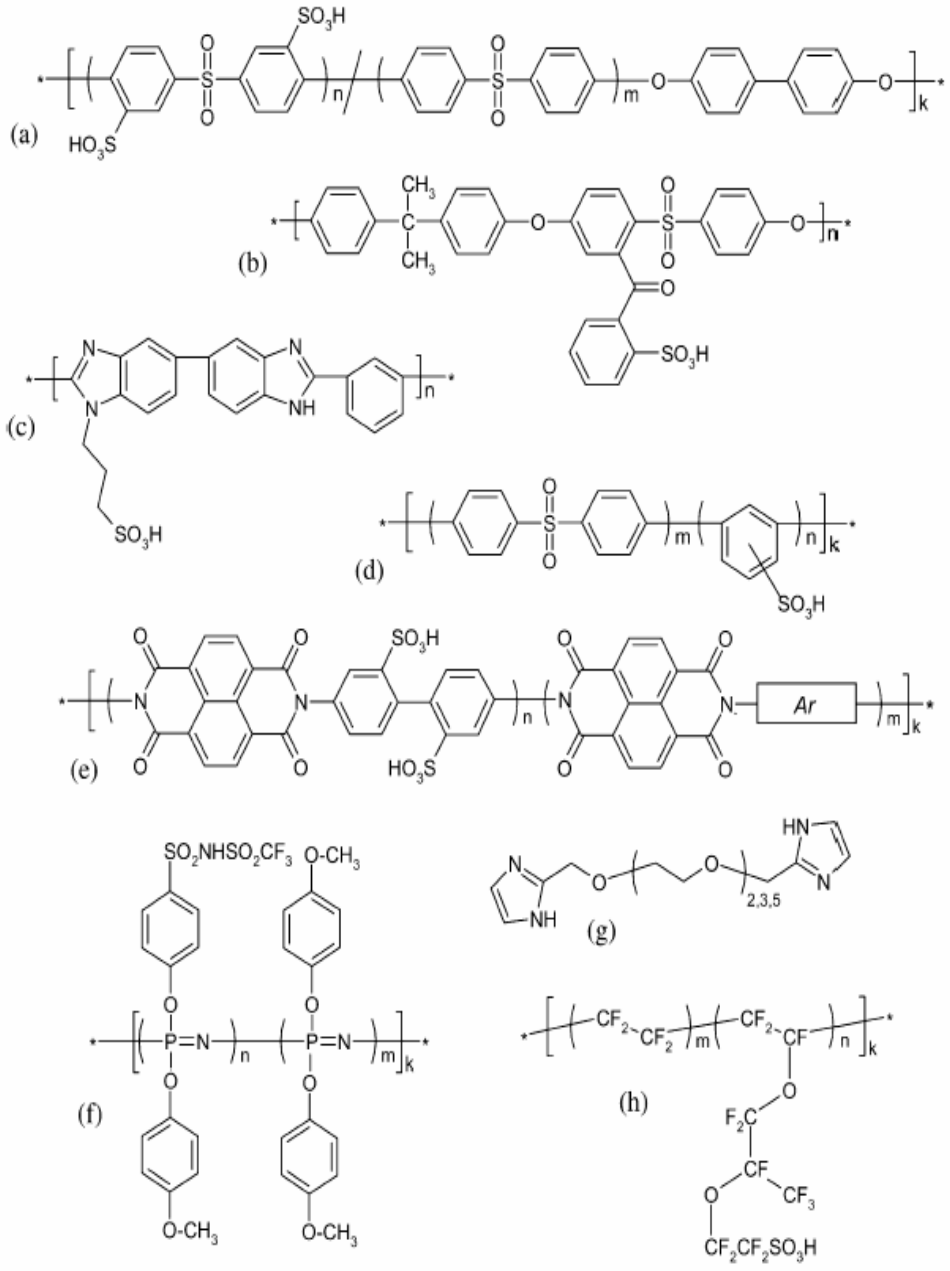

Figure 3.3 Examples of proton conducting polymers currently under investigation as PEM materials: (a) sulfonated poly(arylene ether sulfone) (Wang et al., 2002) (b) sulfophenylated polysulfone (Jannasch et al., 2002); (c) sulfopropylated PBI (Kawahara et al., 2000, Rikukawa et al., 2000; (d) sulfonated poly(arylene-co-arylene sulfone) (Poppe et al., 2002); (e) sulfonated naphthalenic polyimide (Ar, various aromatic moieties) (Genies et al. 2001); (f) poly(aryloxyphosphazene) having sulfonimide units (Hofmann et al., 2002); (g) imidazole-terminated ethylene oxide oligomers (Meyer et al., 2001); and (h) Nafion marketed by the DuPont company.

Poppe et al. have produced flexible PEMs based on carboxylated and sulfonated poly (arylene-co-arylene sulfone)s (Poppe et al., 2002). As expected, the carboxylated materials showed lower water uptake and lower conductivity in comparison with the sulfonated ones. Sulfonated polysulfones have also been blended with basic polymers such as polybenzimidazole (PBI) and poly (4-vinyl pyridine) in order to improve the performance in direct methanol fuel cells (Jönissen et al., 2002).

Different sulfonated aromatic polyimides are also under investigation (Guo et al., 2002, Genies et al., 2001, Mercier et al., 2001, and Besse et al., 2002). These ionomers typically reach high levels of conductivity, but the hydrolytic stability is reported to be very sensitive to the chemical structure of the polyimide main-chain (Genies et al., 2001). A membrane-electrode assembly based on a sulfonated polyimide was recently evaluated in a fuel cell at 70 °C, and was found to have a performance similar to Nafion (Besse et al., 2002).

Sulfonated PBI has been investigated by Kawahara et al. and Asensio et al. (Kawahara et al., 2000, and Asensio et al., 2002). At low water contents, PEMs of PBI grafted with sulfopropyl units showed proton conductivity in the order of 10^{-3} S/cm in the temperature range from 20 to 140 °C, which is superior to Nafion under the same conditions (Kawahara et al., 2000). The performance of these PEMs has also recently been investigated in fuel cells at temperatures up to 150 °C under fully humidified conditions (Bae et al., 2002).

As the operation temperature of the PEMs is increased to temperatures above 100 °C, desulfonation, i.e. loss of the sulfonic acid unit though hydrolysis becomes an increasingly important problem. Acidic moieties having higher stability include phosphonic acid and sulfonimides. The latter is a significantly stronger acid compared to sulfonic acid, which may be especially advantageous at low water contents. Allcock et al. have prepared different poly(aryloxyphosphazene)s functionalized with phenyl phosphonic acid units with the intended use in direct methanol fuel cells (Allcock et al., 2002). Just recently, the same

authors also report on the preparation of poly(aryloxyphosphazene)s having sulfonimide units (Hofmann et al., 2002). Blending and radiation cross linking have been investigated as means to reduce water swelling and methanol permeation of poly(aryloxyphosphazene) ionomers (Carter et al., 2002).

Two different polymer membrane systems based on Nafion and Teflon were investigated as proton conductors for polymer membrane fuel cells (Sun et al., 2001). Water-free Nafion117 membranes swollen with different non-aqueous solvents were prepared. The solvents included imidazole, imidazole–imidazolium salt solutions, room temperature molten salts and molten salt–acid solutions. Teflon films were treated with a surfactant, or a Nafion solution, to improve their surface properties, and were subsequently swollen with phosphoric acid. Conductivity measurements were carried out on both the Nafion and Teflon membranes. The Nafion membranes swelled with the imidazole–imidazolium salt solutions exhibited conductivity in the range of $3–4x10^{-3}$ S/cm around 100°C. This method of producing water-free systems for PEMFC membranes is therefore promising although conductivities need to be improved significantly. For the Nafion membranes swollen with the molten salts or molten salt–acid solutions, their conductivity is not as high as expected, which may be because the molten salts are not very hydrophilic, and could not play an effective role in disassociation of protons from the sulfonyl groups attached to Nafion backbones. The Teflon films treated with the surfactant solution or the Nafion solution presented good compatibility with phosphoric acid, and the Teflon membrane–phosphoric acid systems also exhibited good conductivity at higher temperatures. Further investigation on these systems should include a study of thermal stability and electrochemical stability, as well as testing in a fuel cell device (Sun et al., 2001).

CHAPTER 4

PROTON CONDUCTION

Proton transfer mechanisms are well-established phenomena in nature. Most biochemical reactions are very sensitive to changes in the pH of the surrounding environment so proton transfer serves as a vital route in the cell pH stabilization. In biological systems, while information is generally transferred via metal ions, all processes which convert energy from one form to another involve protonation and deprotonation reactions (Voet D. and Voet J.G., 1992).

Proton conductivity also plays a key role in other important processes as diverse as the photosynthesis in plants to the generation of clean electrical energy in fuel cell power plants. Such as extensive range of proton transport and transfer phenomena has therefore attracted interest from material through understanding of the mechanisms and processes has been established. Hence, the identification and development of new proton conducting materials, especially for the solid electrolyte domain, relies heavily on this collective knowledge.

4.1 PROTON CONDUCTION MECHANISMS

The proton is unique in that it is the only ion which possesses no electronic shell. It therefore strongly interacts with the electron density of its environment. In the case of metals, the proton interacts with the electron density of the conduction band, and is considered to be a hydrogen atom with a protonic or hydridic character. Metals are also unique in that they allow the proton (hydrogen) to have a high coordination number, typically four or six at a tetrahedral or octahedral site (Kreuer, 1988). In non-metallic compounds, the proton interacts strongly with the electron density of only one or two

nearest neighbors. If this is a single oxygen atom, while being well separated from other electronegative species, this results in the formation of an O-H bond which is less than 100 pm in length (Figure 4.1a), compared to ~ 140 pm for the ionic radius of the oxide ion. In this state, the protons equilibrium position lies deeply embedded in the electron density of the oxygen. For medium distances between two oxygen atoms (~ 250-280 pm), the proton may be involved in two bonds: a short, strong bond with a proton donor and a long, weak bond with a proton acceptor. This is the case of an asymmetrical hydrogen bond (O-H…O) which is directional in character (Figure 4.1b). For shorter oxygen separations (~240 pm), a symmetrical hydrogen bond may be formed where the proton is involved in two equivalent bonds (Schuster et al., 1976) (Figure 4.1c).

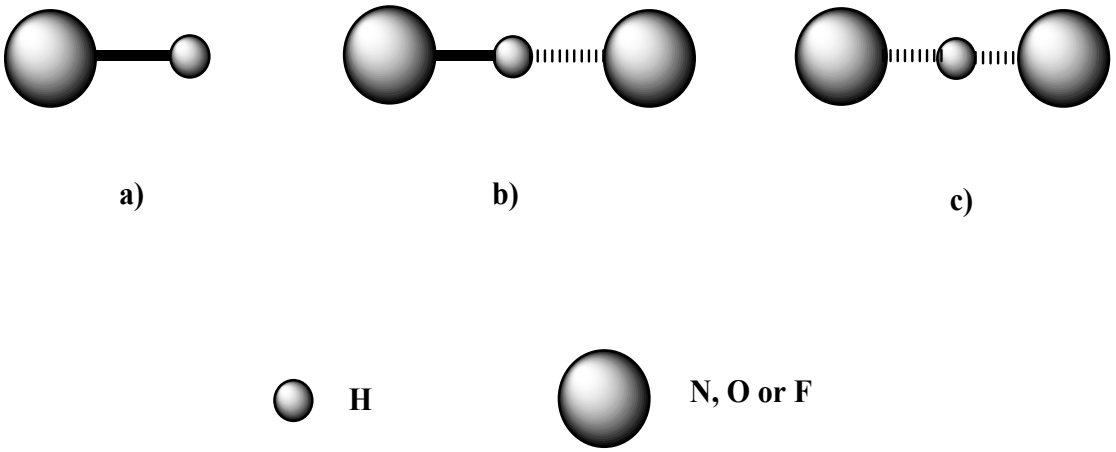

Figure 4.1 Schematic representation showing different classes of proton interaction in a nonmetallic environment with one or two basic entities (Schuster et al., 1976).

Proton transfer phenomena follow two principal mechanisms where the proton remains shielded by electron density along its entire diffusion path, so that in effect the momentary existence of a free proton is not seen. The most trivial case of proton migration requires the translational dynamics of bigger species: this is the vehicle mechanism (Kreuer et al., 1982). In this mechanism the proton diffuses through the medium together with a "vehicle" (for example, with H_2O as H_3O^+). The counter diffusion of unprotonated vehicles (H_2O) allows the net transport of protons. The observed conductivity, therefore, is directly dependant on the rate of vehicle diffusion. In the other principal mechanism, the vehicles show pronounced local dynamics but reside on their sites. The protons are transferred from one vehicle to the other by

hydrogen bonds (proton hopping). Simultaneous reorganization of the proton environment, consisting of reorientation of individual species or even more extended ensembles, then leads in the formation of an uninterrupted path for proton migration. This mechanism is known as the Grotthuss mechanism. This reorganization usually involves the reorientation of solvent dipoles (for example H_2O), which is an inherent part of establishing the proton diffusion pathway. The rates of proton transfer and reorganization of its environment affect directly this mechanism. All rates directly connected to the diffusion of protons are schematically illustrated in Figure 4.2.

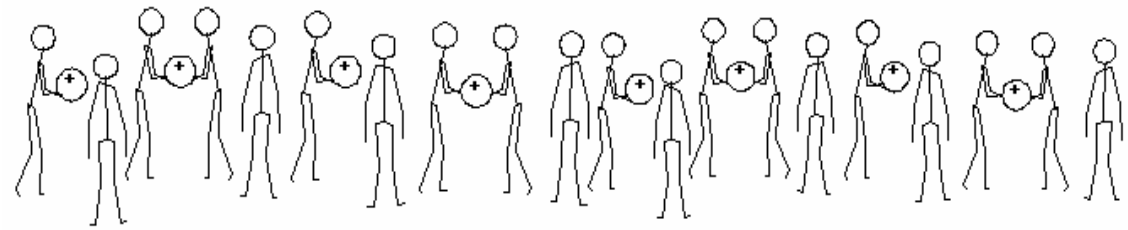

Grotthuss Mechanism

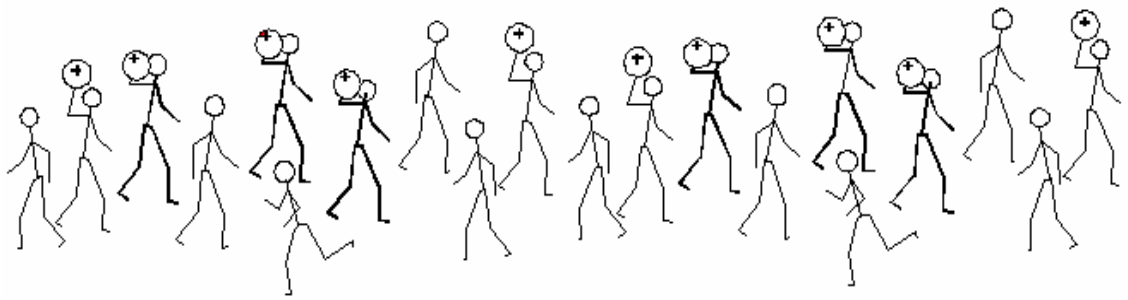

Vehicle Mechanism

Figure 4.2 Schematic representation of phenomena involved in proton conduction mechanisms (Kreuer et al., 1982)

These two principle mechanisms essentially reflect the difference in nature of the hydrogen bonds formed between the protonated species and their environment. In media which supports strong hydrogen bonding, the Grotthuss mechanism is preferred; the vehicle mechanism is characteristic of species with weaker bonding.

CHAPTER 5

APPLICATION OF PROTON CONDUCTING ELECTROLYTES

5.1 FUEL CELLS

Fuel cells are electrochemical devices that convert the chemical energy of a reaction directly into electrical energy. The basic physical structure or building block of a fuel cell consists of an electrolyte layer in contact with a porous anode and cathode on either side. A schematic representation of a fuel cell with the reactant/product gases and the ion conduction flow directions through the cell is shown in Figure 5.1.

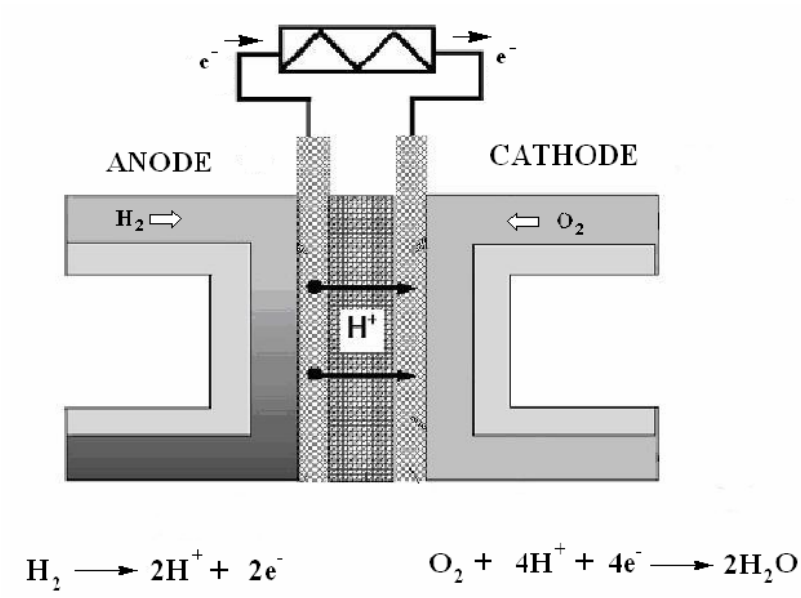

Figure 5.1 Schematic of an Individual Fuel Cell (Fuel Cell Handbook, 2000)

In a typical fuel cell, gaseous fuels are fed continuously to the anode (negative electrode) compartment and an oxidant (i.e., oxygen from air) is fed continuously to the cathode (positive electrode) compartment; the electrochemical reactions take place at the electrodes to produce an electric current. A fuel cell, although having components and characteristics similar to those of a typical battery, differs in several respects. The battery is an energy storage device. The maximum energy available is determined by the amount of chemical reactant stored within the battery itself. The battery will cease to produce electrical energy when the chemical reactants are consumed (i.e., discharged). In a secondary battery, the reactants are regenerated by recharging, which involves putting energy into the battery from an external source. The fuel cell, on the other hand, is an energy conversion device that theoretically has the capability of producing electrical energy for as long as the fuel and oxidant are supplied to the electrodes. Figure 5.2 is a simplified diagram that demonstrates how the fuel cell works. In reality, degradation, primarily corrosion, or malfunction of components limits the practical operating life of fuel cells.

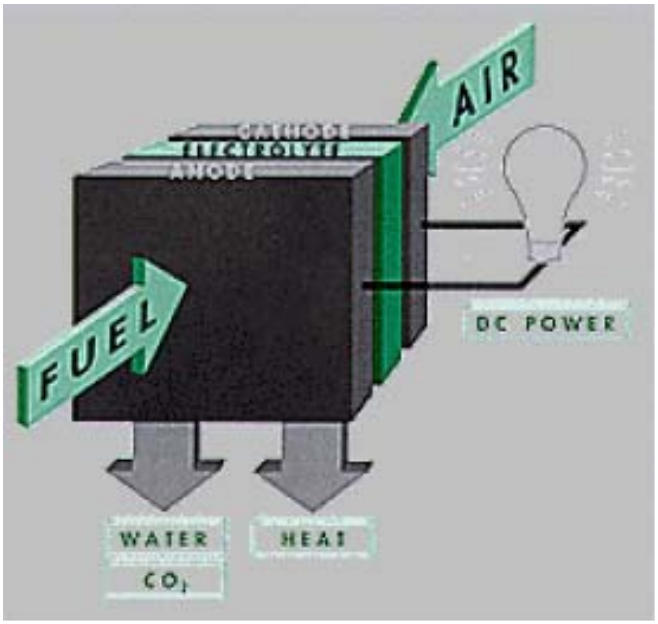

Figure 5.2 Simplified Fuel Cell Schematic (Fuel Cell Handbook, 2000)

Note that the ion specie and its transport direction can differ, influencing the site of water production and removal, a system impact. The ion can be either a positive or a

negative ion, meaning that the ion carries either a positive or negative charge (surplus or deficit of electrons). The fuel or oxidant gases flow past the surface of the anode or cathode opposite the electrolyte and generate electrical energy by the electrochemical oxidation of fuel, usually hydrogen, and the electrochemical reduction of the oxidant, usually oxygen. In theory, any substance capable of chemical oxidation that can be supplied continuously (as a fluid) can be burned galvanically as the fuel at the anode of a fuel cell (Appleby and Foulkes, 1989)

Similarly, the oxidant can be any fluid that can be reduced at a sufficient rate. Gaseous hydrogen has become the fuel of choice for most applications, because of its high reactivity when suitable catalysts are used, its ability to be produced from hydrocarbons for terrestrial applications, and its high energy density when stored cryogenically for closed environment applications, such as in space. Similarly, the most common oxidant is gaseous oxygen, which is readily and economically available from air for terrestrial applications, and again easily stored in a closed environment. A three-phase interface is established among the reactants, electrolyte, and catalyst in the region of the porous electrode. The nature of this interface plays a critical role in the electrochemical performance of a fuel cell, particularly in those fuel cells with liquid electrolytes. In such fuel cells, the reactant gases diffuse through a thin electrolyte film that wets portions of the porous electrode and react electrochemically on their respective electrode surface. If the porous electrode contains an excessive amount of electrolyte, the electrode may "flood" and restrict the transport of gaseous species in the electrolyte phase to the reaction sites. The consequence is a reduction in the electrochemical performance of the porous electrode. Thus, a delicate balance must be maintained among the electrode, electrolyte, and gaseous phases in the porous electrode structure. Much of the recent effort in the development of fuel cell technology has been devoted to reducing the thickness of cell components while refining and improving the electrode structure and the electrolyte phase, with the aim of obtaining a higher and more stable electrochemical performance while lowering cost (Fuel Cell Handbook, 2000)

The electrolyte not only transports dissolved reactants to the electrode, but also conducts ionic charge between the electrodes and thereby completes the cell electric

circuit. It also provides a physical barrier to prevent the fuel and oxidant gas streams from directly mixing.

The functions of porous electrodes in fuel cells are: 1) to provide a surface site where gas/liquid ionization or de-ionization reactions can take place, 2) to conduct ions away from or into the three phase interface once they are formed (so an electrode must be made of materials that have good electrical conductance), and 3) to provide a physical barrier that separates the bulk gas phase and the electrolyte. A corollary of item 1 is that, in order to increase the rates of reactions, the electrode material should be catalytic as well as conductive, porous rather than solid. The catalytic function of electrodes is more important in lower temperature fuel cells and less so in high temperature fuel cells because ionization reaction rates increase with temperature. It is also a corollary that the porous electrodes must be permeable to both electrolyte and gases, but not such that the media can be easily "flooded" by the electrolyte or "dried" by the gases in a one-sided manner (Fuel Cell Handbook, 2000).

A variety of fuel cells are in different stages of development. They can be classified by use of diverse categories, depending on the combination of type of fuel and oxidant, whether the fuel is processed outside (external reforming) or inside (internal reforming) the fuel cell, the type of electrolyte, the temperature of operation, whether the reactants are fed to the cell by internal or external manifolds, etc. The most common classification of fuel cells is by the type of electrolyte used in the cells and includes 1) polymer electrolyte fuel cell (PEFC), 2) alkaline fuel cell (AFC), 3) phosphoric acid fuel cell (PAFC), 4) molten carbonate fuel cell (MCFC), 5) intermediate temperature solid oxide fuel cell (ITSOFC), and 6) tubular solid oxide fuel cell (TSOFC). These fuel cells are listed in the order of approximate operating temperature, ranging from ~80 °C for PEFC, ~100 °C for AFC, ~200 °C for PAFC, ~650 °C for MCFC, ~800 °C for ITSOFC, and 1000 °C for TSOFC. The operating temperature and useful life of a fuel cell dictate the physicochemical and thermo mechanical properties of materials used in the cell components (i.e., electrodes, electrolyte, interconnect, current collector, etc.). Aqueous electrolytes are limited to temperatures of about 200 °C or lower because of their high water vapor pressure and/or rapid degradation at higher temperatures. The operating temperature also plays an important role in dictating the type of fuel that can be used in a fuel cell. The low-temperature fuel cells with aqueous electrolytes are, in

most practical applications, restricted to hydrogen as a fuel. In high-temperature fuel cells, CO and even CH_4 can be used because of the inherently rapid electrode kinetics and the lesser need for high catalytic activity at high temperature. However, descriptions later in this section note that the higher temperature cells can favor the conversion of CO and CH_4 to hydrogen then use the equivalent hydrogen as the actual fuel.

5.1.1 Polymer Electrolyte Fuel Cell (PEFC)

The electrolyte in this fuel cell is an ion Exchange membrane (fluorinated sulfonic acid polymer or other similar polymer) that is an excellent proton conductor. The only liquid in this fuel cell is water; thus, corrosion problems are minimal. Water management in the membrane is critical for efficient performance; the fuel cell must operate under conditions where the byproduct water does not evaporate faster than it is produced because the membrane must be hydrated. Because of the limitation on the operating temperature imposed by the polymer, usually less than 120 °C, and because of problems with water balance, a H_2-rich gas with minimal or no CO (a poison at low temperature) is used. Higher catalyst loading (Pt in most cases) than that used in PAFCs is required for both the anode and cathode (Fuel Cell Handbook, 2000).

5.1.2 Alkaline Fuel Cell (AFC)

The electrolyte in this fuel cell is concentrated (85 wt %) KOH in fuel cells operated at high temperature (~250 °C), or less concentrated (35-50 wt %) KOH for lower temperature (<120 °C) operation. The electrolyte is retained in a matrix (usually asbestos), and a wide range of electrocatalysts can be used (e.g., Ni, Ag, metal oxides, spinels, and noble metals). The fuel supply is limited to non-reactive constituents except for hydrogen. CO is a poison, and CO_2 will react with the KOH to form K_2CO_3, thus altering the electrolyte. Even the small amount of CO_2 in air must be considered with the alkaline cell (Fuel Cell Handbook, 2000).

5.1.3 Phosphoric Acid Fuel Cell (PAFC)

Phosphoric acid concentrated to 100 % is used for the electrolyte in this fuel cell, which operates at 150 to 220 °C. At lower temperatures, phosphoric acid is a poor ionic conductor, and CO poisoning of the Pt electrocatalyst in the anode becomes severe. The relative stability of concentrated phosphoric acid is high compared to other common acids; consequently the PAFC is capable of operating at the high end of the acid temperature range (100 to 220 °C). In addition, the use of concentrated acid (100 %) minimizes the water vapor pressure so water management in the cell is not difficult. The matrix universally used to retain the acid is silicon carbide and the electrocatalyst in both the anode and cathode is Pt (Fuel Cell Handbook, 2000).

5.1.4 Molten Carbonate Fuel Cell (MCFC)

The electrolyte in this fuel cell is usually a combination of alkali carbonates, which is retained in a ceramic matrix of $LiAlO_2$. The fuel cell operates at 600 to 700 °C where the alkali carbonates form a highly conductive molten salt, with carbonate ions providing ionic conduction. At the high operating temperatures in MCFCs, Ni (anode) and nickel oxide (cathode) are adequate to promote reaction. Noble metals are not required (Fuel Cell Handbook, 2000).

5.1.5 Intermediate Temperature Solid Oxide Fuel Cell (ITSOFC)

The electrolyte and electrode materials in this fuel cell are basically the same as used in the TSOFC. The ITSOFC operates at a lower temperature, however, typically between 600 to 800 °C. For this reason, thin film technology is being developed to promote ionic conduction; alternative electrolyte materials are also being developed (Fuel Cell Handbook, 2000).

5.1.6 Tubular Solid Oxide Fuel Cell (TSOFC)

The electrolyte in this fuel cell is a solid, nonporous metal oxide, usually Y_2O_3-stabilized ZrO_2. The cell operates at 1000° C where ionic conduction by oxygen ions takes place. Typically, the anode is Co-ZrO_2 or Ni-ZrO_2 cermet, and the cathode is Sr-

doped $LaMnO_3$. In low-temperature fuel cells (PEFC, AFC, and PAFC), protons or hydroxyl ions are the major charge carriers in the electrolyte, whereas in the high-temperature fuel cells, MCFC, ITSOFC, and TSOFC, carbonate ions and oxygen ions are the charge carriers, respectively. Major differences between the various cells are shown in Table 5.1 (Fuel Cell Handbook, 2000).

Table 5.1. Summary of Major Differences of the Fuel Cell Types (Fuel Cell Handbook, 2000)

	PEFC	**AFC**	**PAFC**	**MCFC**	**ITSOFC**	**TSOFC**
Electrolyte	Ion Exchange Membranes	Mobilized or Immobilized Potassium Hydroxide	Immobilized Liquid Phosphoric Acid	Immobilized Liquid Molten Carbonate	Ceramic	Ceramic
Operating Temperature	80°C	65-220°C	205°C	650°C	600-800°C	800-1000°C
Charge Carrier	H^+	OH^-	H^+	CO_3^{2-}	O^{2-}	O^{2-}
External Reformer for CH_4 (below)	Yes	Yes	Yes	No	No	No
Prime Cell Components	Carbon-based	Carbon-based	Graphite-based	Stainless-based	Ceramic	Ceramic
Catalyst	Platinum	Platinum	Platinum	Nickel	Perovskites	Perovskites
Product Water Management	Evaporative	Evaporative	Evaporative	Gaseous Product	Gaseous Product	Gaseous Product
Product Heat Management	Process Gas + Independent Cooling Medium	Process Gas + Electrolyte Calculation	Process Gas + Independent Cooling Medium	Internal Reforming + Process Gas	Internal Reforming + Process Gas	Internal Reforming + Process Gas

5.2 ELECTROCHROMISM AND SMART WINDOWS

An electrochromic device (ECD) is able to modify its optical absorption in a reversible and persistent way with the application of a voltage. Electrochromism is a term that is used to describe the fact that certain materials change color when their composition is changed by use of an electrochemical cell. Based on this principle, windows and mirrors utilizing these materials can be reversibly colored or bleached (Tillement, 1994).

ECDs have numerous potential applications in technology. Thus, the possibility to modulate the diffuse reflectance lends itself to non-emissive display devices of different

sizes. Modulation of the specular reflectance opens possibilities for anti-dazzling rear view mirrors for automobiles and innovative architecture. Passenger cars with EC-based compartment rear-view mirrors have been available on the market for a few years.

Modulation of the luminous transmittance can be used in future buildings for superior day lighting and hence good working conditions, with a minimum electric lighting. Other application may be for sun glasses and also for windows in cars, trains, ships, etc. Smart windows, of the types referred to here are not yet on the market, but a growing awareness of the imminent dangers of energy use is the source fossil or nuclear is bound to lead to an increased interest in smart windows or other solar energy related technologies (Granqvist, 1992).

Such an electrochromic device that operates in the transmission mode can consist of a galvanic cell with several different layers (Figure 5.3):

(a) A transparent electrically conducting film on the glass substrate
(b) A thin film of an electrochromic material
(c) An electrolyte in liquid or perfectly solid form
(d) A counter electrode operating in conjunction with the electrochromic material
(e) An electrically conducting, transparent back electrode

All component layers are transparent in the uncolored state and the coloration should be reversible. The coloration of the electrochromic layer can be achieved by passing current through the cell. The degree of coloration can be controlled by the amount of charge passed through the cell and the colored state remains after switching of the voltage. To bleach the device, one just needs to reverse the polarity of the voltage.

The EC material and counter electrode are mixed conductors for electrons and ions. The materials showing electrochromic properties include organic compounds and inorganic compounds. Most well-known electrochromic materials are shown in Table 5.2. In order for the utilizing, electrochromic materials are processed into the thin film.

Table 5.2 Most well-known electrochromic materials

	Inorganic	Organic
Cathodic	WO_3, MoO_3, TiO_2, …	…
Anodic	NiO_2, IrO_2, RhO_2, …	Polyaniline, Polypyyrole, Prussian blue, …

The electrochromic redox reactions result in the coloring and bleaching of WO_3 (eq.5.1)

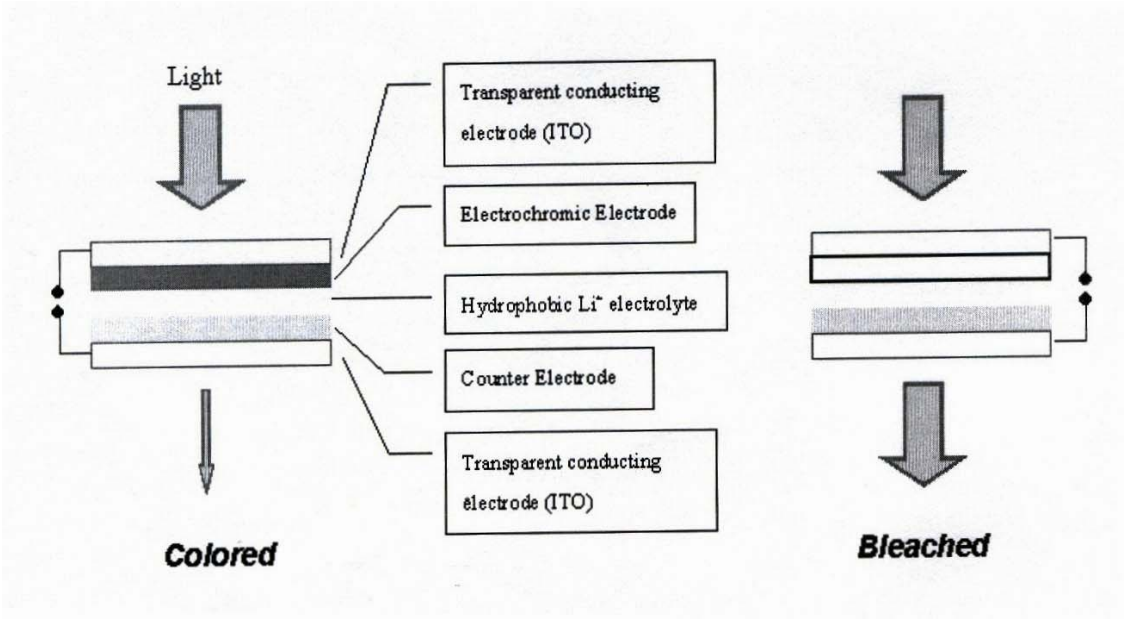

Figure 5.3 Basic design of an ECD, indicating the transport of protons under the action of an electric field (Tillement, 1994)

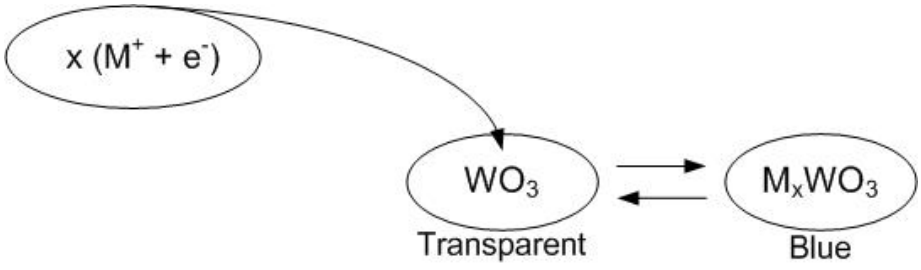

(5.1)

Depending on the electrolyte the ions can be H^+, Li^+, Na^+, K^+, H_3O^+, and OH^- or the complexes of them (Goldner et al., 1992, Goldner et al., 1988, Ohno and Yamazaki, 1993). The solid electrolyte can be either inorganic, such as hydrated oxide film, or organic (polymer). The requirements of the electrolyte are as follows:

(a) An ionic conductivity larger than a value between 10^{-4}-10^{-5} S/cm, depending on the application
(b) Electronic conductivity less than $1x10^{-12}$ S/cm
(c) Electrochemical stability for extended cycling temperature and, during UV irradiation
(d) Good adherence to adjoining materials

Several proton and ion conducting such as $Na^+$and K^+ polymers for application in these devices have been published (Ohno and Yamazaki, 1993).

CHAPTER 6

EXPERIMENTAL

6.1 PURPOSE AND PREVIEW

To prepare novel anhydrous proton conducting polymer electrolytes satisfying the following requirements:

a) Wide thermal stability window (0~150 ºC), thermodynamic stability, and electrochemical stability
b) Sufficient proton conductivity (~10^{-4} S/cm)

6.2 CHEMICALS

The utilized solvents are obtained from the companies Aldrich, Fluka and Merck with P.A. reagent quality. Commercial alginic acid (molecular weight 240 kDa) which contains approximately 61 % mannuronic acid and 39 % gluronic acid was obtained from Sigma. Poly(vinylphosphonic acid), PVPA was received from Polysciences and has an average molecular weight of 20,000 g/mol. 2-acryl amido-2-methylpropanesulfonic acid, AMPSA (> 98 %) and 1H- 1,2,4-triazole ,Tri, with melting point: 120 ^{o}C , boiling point: 260 ^{o}C is a crystalline solid at room temperature are obtained from Aldrich.

6.3 SYNTHESIS OF HOMOPOLYMERS

PAMPSA was produced by free radical polymerization technique. The addition of a monomer molecule to an active chain end regenerates the active site at the chain end.

Hence, a large number of monomer molecules are ‘consumed’ for each active site introduced into the system. In chain reaction, four distinct types of processes are recognized.

a) Chain Initiation: A process in which highly reactive transient molecules or active centers are formed.

b) Chain Propagation: The addition of monomer molecules to the active chain end, accompanied by regeneration of the terminal active site.

c) Chain Transfer: Involving the transfer of the active site to another molecule (e.g., monomer). The molecule that has lost the active site is now “dead” from a chain propagation point of view. The molecule that has accepted the active site can start a new chain.

d) Chain Termination: A reaction in which the active chain centers are destroyed. Chain reactions are found in free radical, anionic and cationic vinyl type polymerizations. In-free radical process all of the four steps listed above can usually be identified.

Schematically, a free-radical polymerization sequence can be represented by reactions shown in equation 6.1. In this equation, M represents a molecule of monomer; R’· is an initiating free radical from the initiator; R_n is the propagating free radical with a degree of polymerization, n; YZ is a chain transfer agent that may be solvent, monomer, initiator, or polymer molecules; and P_n is the final inactive polymer. It should be noted that in some cases the initiator molecule may be the monomer itself.

$$
\begin{array}{lll}
\text{Initiator} \longrightarrow 2R'\cdot & & \\
R'\cdot + M \longrightarrow R_1\cdot & \left.\right\} & \text{Initiation} \\
R_i\cdot + M \longrightarrow R_2\cdot & & \\
\cdots\cdots\cdots\cdots & \left.\right\} & \text{Propagation} \\
R_n\cdot + M \longrightarrow R_{n+1}\cdot & & \\
R_n\cdot + YZ \longrightarrow R_nY + Z\cdot & & \text{Chain Transfer} \\
R_n\cdot + R_m\cdot \longrightarrow P_{n+m} & \left.\right\} & \text{Termination} \\
R_n\cdot + R_m\cdot \longrightarrow P_n + P_m & &
\end{array}
\qquad \textbf{(6.1)}
$$

6.3.1 The Synthesis of Homopolymer

6.3.1.1 The Synthesis of PAMPSA

PAMPSA was produced by free radical polymerization of 2-acrylamido-2-methyl-1 propanesulfonic acid in 1,4-dioxane:deionized water 2 to1 stoichiometric ratio in which 1% potassium persulfate by weight (relative to mass of the monomer) was used as an initiator. The reaction mixture was purged with nitrogen and the polymerization reaction was performed at 70 ºC for 36 h. Aqueous solution of the polymer was precipitated in ethanol and the product was dried at 50 ºC under vacuum. The product was brittle at ambient temperature (Figure 6.1).

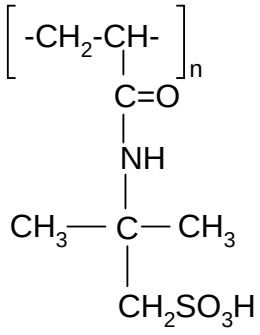

Figure 6.1 Structure of poly(2-acrylamido-2-methyl-1-propanesulfonic acid)

6.4 PREPARATION OF BLENDS

6.4.1 Preparation of PAMPSATri$_x$ Blends

The stoichiometric amount of PAMPSATri (1, 2) blends which was prepared by mixing of PAMPSA in water, then Tri was added and the solution was stirred overnight. After obtaining a homogeneous mixture, the gels were cast on Teflon® plates and dried at 50 ^{o}C under atmospheric pressure, then further dried under vacuum during 24 h. Transparent, homogeneous films were obtained with a thickness ranging from 50 to 150 μm. Similar procedures were followed for the preparation of other compositions.

6.4.2 Preparation of PVPATri$_x$ Blends

The preparation of PVPATri$_1$ complex electrolyte is as follows: 1g of PVPA (Fig. 6.2) was dissolved in water, then 0.63 g (9 mmol) Tri (Fig. 6.2) was admixed and the solution was stirred for 24 h to make it homogeneous. Then the solutions were cast on Teflon® plates and dried at 50 ^{o}C under nitrogen atmosphere and afterward the films further dried under vacuum. Homogeneous and thin films were obtained for all the blends.

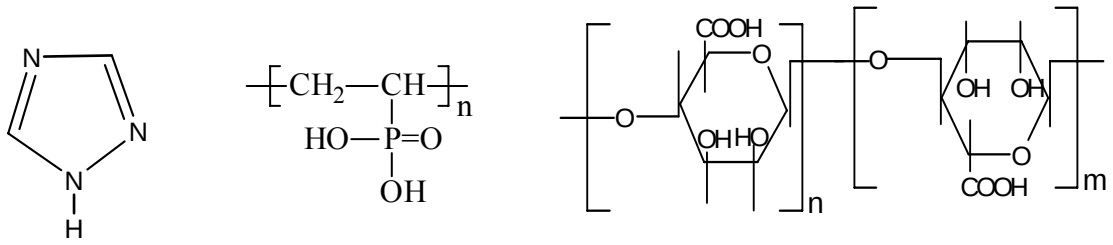

Tri PVPA AL

Figure 6.2 Molecular structures of AL, PVPA, and Tri.

6.4.3 Preparation of ALTri$_x$ Blends

The receipt of preparation of ALTri$_1$ complex electrolytes is as follows: 1 g of AL (Fig. 6.2) was dissolved in 10 ml of water, then 0.392 g (6 mmol) Tri was admixed and the solution was stirred overnight. After obtaining a homogeneous mixture, the gels were cast on Teflon® plates and dried at 50 ^{o}C under atmospheric pressure, then further dried under vacuum at the same temperature during 24 h. Transparent, homogeneous films were obtained with a thickness ranging from 50 to 100 μm (Fig. 6.3). Similar procedures were followed for the preparation of other compositions. ALTri$_x$ (x = 1.5) is the maximum mixing level above which the materials lost their transparency and become heterogeneous.

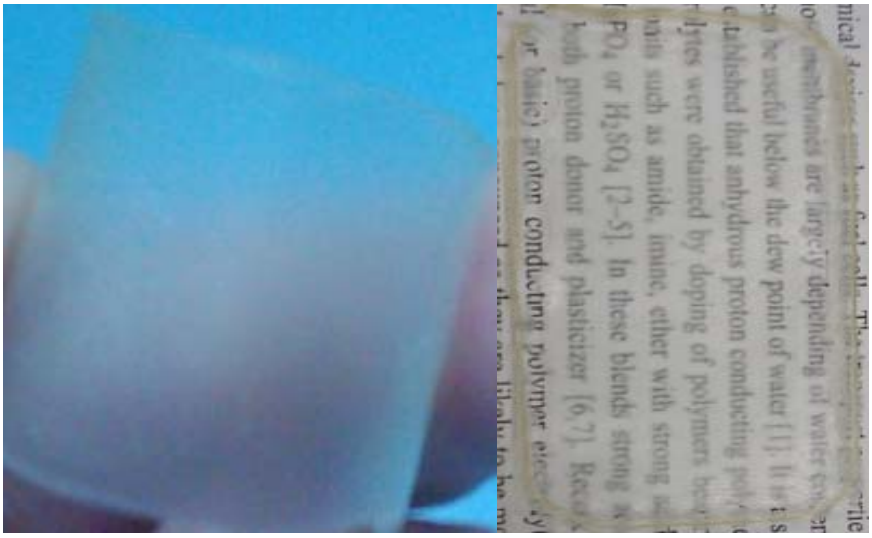

Figure 6.3 Appearance of $AlTri_{l,}$ the free standing film (3.5 cm x 7 cm)

The composite electrolytes, which are known in many embodiments, face the problem that low molecular weight may be washed out during fuel cell operation (Xing and Savadogo, 2005). Therefore in the current system, $ALTri_x$ electrolytes were immersed in methanol at various periods of time and the weight change was recorded with time. As it is shown in Figure 6.4, the materials with x = 0.5 and x = 1 exhibited good Triazole-retention capability and maintained their weights. This can be attributed to formation of complexes up on blending of the biopolymer with triazole. However, at higher doping ratios ($x \geq 1.5$), the weight loss becomes more pronounced which is probably due to leaching out of the excess dopant from the film. The weight change was analyzed by weighting the vacuum dried films.

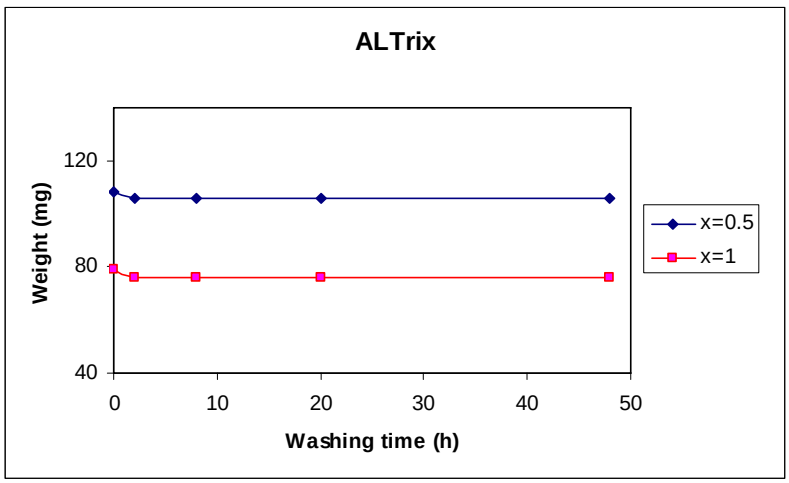

Figure 6.4 Triazole washing out after immersion of the $ALTri_x$ films in methanol at various times.

6.5 INSTRUMENTATION AND PROCEDURE

TGA Thermal stabilities of polymers and doped electrolytes were investigated by Perkin Elmer Pyris 1 and by TGA Mettler TG50, respectively. The samples (~ 10mg) were heated with a rate of 10 ºC/min from room temperature to 700 ºC under an inert atmosphere.

DSC data were obtained between -150/+150 ^{o}C using Mettler-Toledo DSC 30 instrument. The samples are weighted (10-15 mg) and loaded into aluminum pans and slowly cooled from room temperature to starting temperature. Samples were then heated to desired temperature with a scan rate of 10 ^{o}C/min (Run I). In Run II samples were slowly cooled 60-70 ^{o}C below their glass transition temperature then heated to desired temperature. The second heating curves are evaluated. Empty aluminum pans are used as a reference.

FT-IR spectra of the samples were recorded by depositing a thin film onto silicon wafers. The IR spectra (4000-400 cm $^{-1}$ with resolution of 4 cm $^{-1}$) have been recorded with Matson Genesis II spectrometer. Complexation of different acidic polymers as a function of triazole was recorded by this technique.

The AC conductivities of the samples were measured in the Max-Plank Institute for Polymer Research using a Novocontrol impedance spectrometer in the frequency range from 1Hz to 1 MHz as a function of temperature. The hot pressed pellets of the samples with a diameter of 10 mm and thickness of about 0.2-0.3 mm were sandwiched between two gold-coated electrodes (Figure 6.5) and their conductivities were measured with 10 ^{o}C intervals under dry-nitrogen atmosphere.

The DC conductivities were obtained by linear fitting of the AC conductivities measurements.

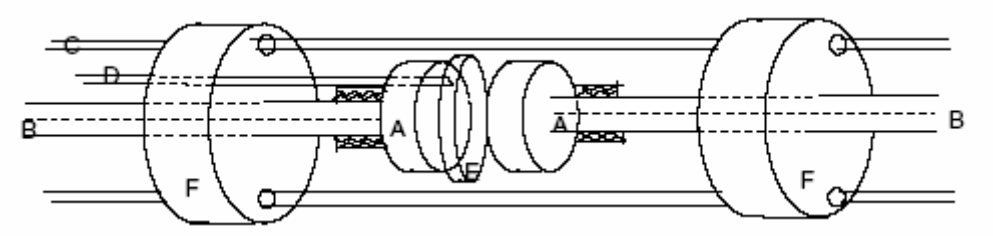

Figure 6.5 Schematic drawing of conductivity cell. (A) Gold plated electrodes, (B) platinum wire, (C) adjustable Hylam screws, (D) thermocouple, (E) membrane, (F) PTFE disks (Smitha et al., 2005).

CHAPTER 7

CHARACTERIZATION OF PROTON CONDUCTING POLYMER ELECTROLYTES

7.1 FT-IR

FT-IR spectroscopy is a powerful tool for structure elucidation. The position, intensity, and shape of vibrational bands are useful in clarifying conformational and environmental changes of polymers at the molecular level.

FT-IR has found particularly wide application in the field of the polymer analysis, not only because of the ability to look at intractable, thick, intensely absorbing materials but also because of the ability to observe chemical and physical changes in the polymer structure with the admixture of the additives (Compell and White, 1989).

7.1.1 FT-IR of PAMPSA and PAMPSATri$_x$ Blends

FT-IR spectra of polymer blends of PAMPSA with various composition of triazole are compared in Figure 7.1. The homopolymer exhibits characteristic absorptions at about 1650 cm^{-1} (amide I) and 1551 cm^{-1} (amide II). Moreover, a strong absorption peak at 1033 cm^{-1} belong to asymmetric O=S=O stretching vibration and broad bond 1218 cm^{-1} due to symmetric O=S=O stretching of the same group (Erdemi et al., 2004). The protonation of the triazole rings from free nitrogen of the heterocycle is proved by the N-H stretch at 3100 cm^{-1}. Additionally, broad bands appearing near 1943 cm^{-1} confirms the presence of quaternary ammonium groups in the polymer electrolytes. The broad absorption in the region of 833–978 cm^{-1} is additional evidence

of the salt formation. Broadening in the region of 3400-2300 cm^{-1} indicates hydrogen bonding network formation.

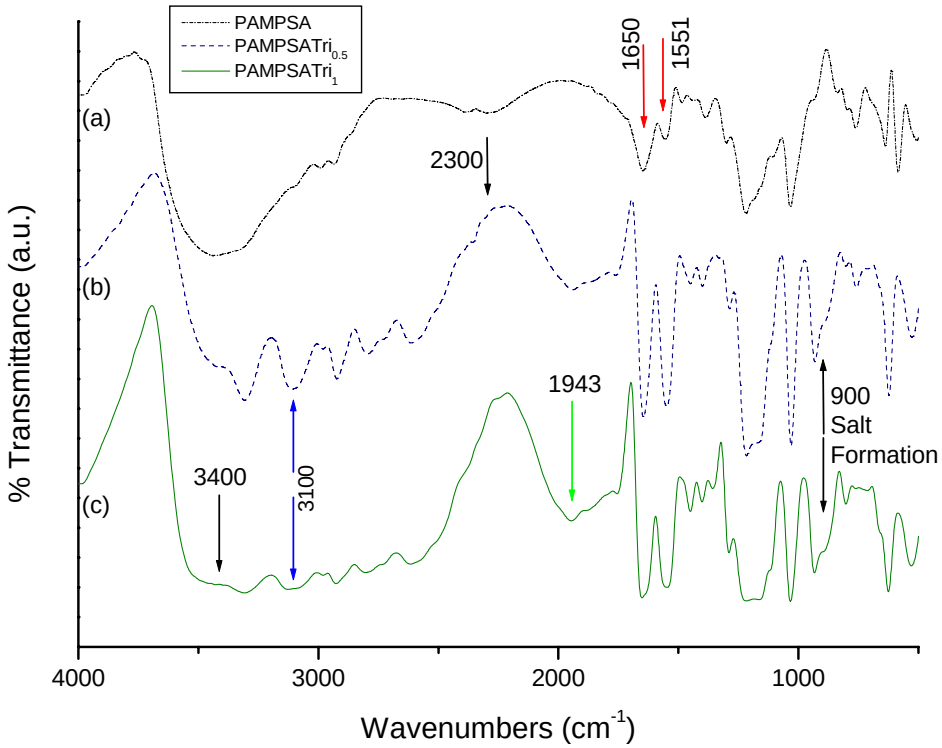

Figure 7.1 FT-IR spectra of homopolymer, PAMPSA (a) and blends: $PAMPSATri_{0.5}$ (b) $PAMPSATri_1$ (c).

7.1.2 FT-IR of PVPA and $PVPATri_x$ Blends

FT-IR spectra of the PVPA and its blends $PVPATri_x$ are represented in Fig 7.2. The spectrum of the PVPA shows broad bands centered at ca. 1000 cm^{-1} and 1140cm^{-1} due to (P-O)H and P=O stretching. The phosphonic acid group gives an additional broad band at 1630 cm^{-1}. The broad band in the region of 3300-2600 cm^{-1} belongs to -OH stretching of the same group. The comparison of the spectra of the homopolymer with blends confirmed the proton exchange reactions after blending. This can be signified by the absorption at 1574 cm^{-1} that corresponds to the protonated triazole ring. The $P\text{-}O^-$ band at 926 cm^{-1} proves the deprotonation of phosphonic acid groups. In addition, the intensity of the N-H stretching band at 3140 cm^{-1} relatively increased with

x due to protonation of the heterocyclic ring. Similar results were suggested for polymer-imidazole hybrid electrolytes

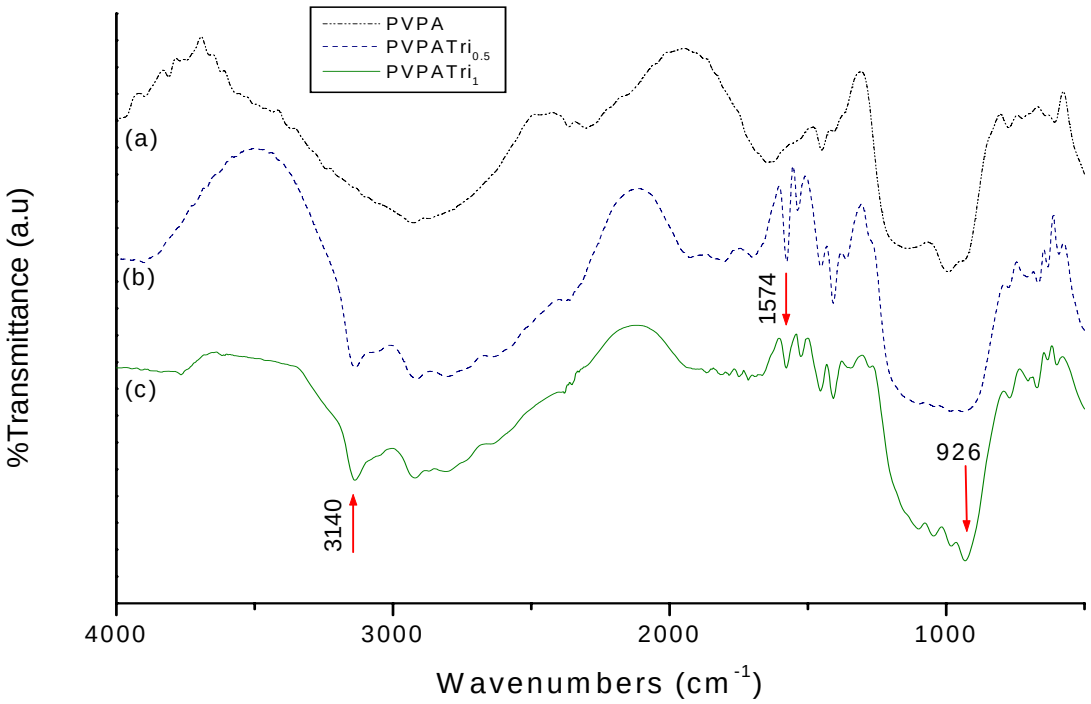

Figure 7.2 FT-IR spectra of homopolymer, PVPA (a) and blends: $PVPATri_{0.5}$ (b) $PVPATri_1$ (c).

7.1.3 FT-IR of AL and $ALTri_x$ Blends

Figure 7.3 presents the FT-IR spectra of the commercial alginic acid and complex electrolytes. The prominent bands at 1731 cm^{-1} and 1628 cm^{-1} are assigned to C=O stretching of carboxylic acid unit of AL (Huang et al., 1999). The band at 1410 cm^{-1} can be ascribed to deformation of the CH_2 units. The saccharide structure gives rise to C-O-C and C-OH stretching in the region of 1200-1290 cm^{-1} and 1000-1100 cm^{-1} (Sartori et al. 1997). When Al is complexed with Tri, the intensity of C=O stretching at 1731 cm^{-1} decreased and peak at 1628 cm^{-1} disappeared. Moreover, new peaks appeared at 1593 cm^{-1} and 1278 cm^{-1} is assigned to asymmetric and symmetric stretching of $-CO_2^-$ units, respectively. Additionally, broad bands appearing near 2400 cm^{-1} and 2000 cm^{-1} confirms the presence of quaternary ammonium groups in the complex electrolytes. The

intensity of N-H stretching peak at 3135 cm^{-1} also increases due to protonation of heterocyclic ring. From these results, it can be concluded that the proton exchange occurs between carboxylic acidic unit and triazole with the result of salt formation.

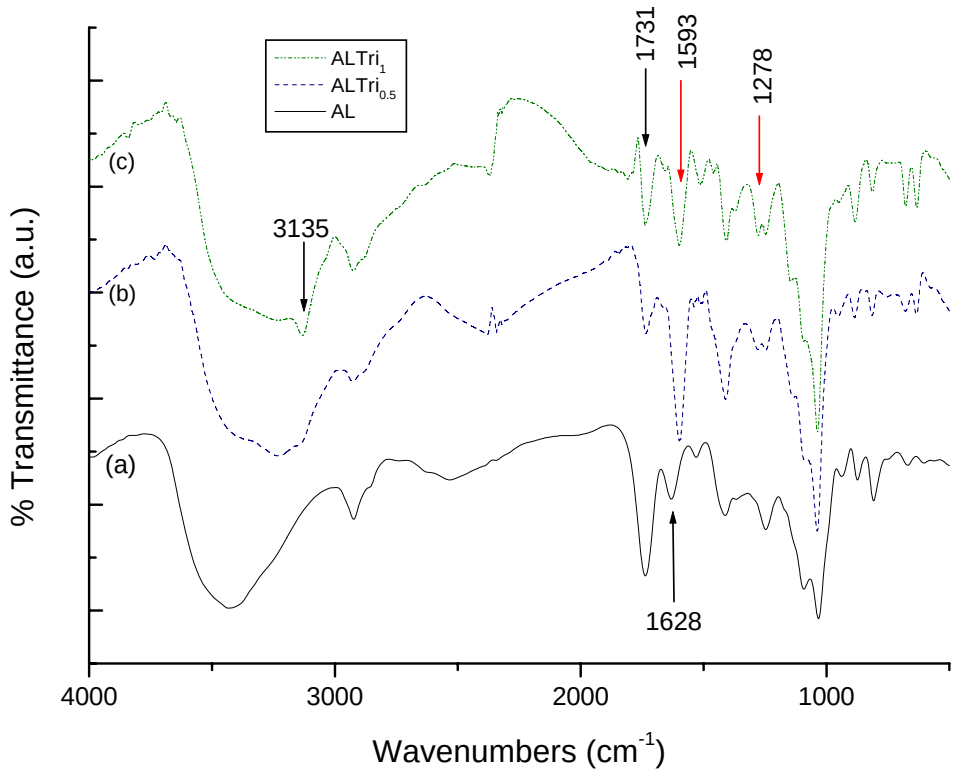

Figure 7.3 FT-IR spectra of the biopolymer and composite electrolytes, AL (a), $ALTri_{0.5}$ (b), and $ALTri_1$ (c).

7.2. X-RAY DIFFRACTION

The separation of amorphous and crystalline contributions in diffraction and spectroscopic data is a necessary step in the study of the structure of the less-ordered regions and in the calculation of crystallinity of a semicrystalline polymer. It is suggested that the diffraction pattern of a polymer with a high degree of crystalline order be fitted with easily resolvable crystalline peaks, and the intensity mot attributable to the crystalline peaks be regarded as amorphous scattering. This amorphous halo can be used as a template in analyzing the diffraction patterns of less-crystalline samples, and to follow changes in the amorphous regions. This method is most useful for

polymers for which a completely amorphous sample cannot be easily prepared, and in the analysis of poorly crystallized polymers (Murthy and Minor, 1990).

7.2.1 X-Ray Diffraction of AL and ALTri$_x$ Blends

Figure 7.4 shows the X-ray diffraction patterns of alginic acid and complex electrolytes. AL exhibits broad peaks around $2\theta = 14^o$ and 21^o which can be attributed to the amorphous structure. For ALTri$_{1.5,}$ the peak at 14^o almost disappeared and at 21^o become more intense as the complex formed between AL and Tri. These results showed that the difference in the intensities of the peaks for each composition reflects the sequential structure of complex electrolytes and ALTri$_{1.5}$ has a greater ordered morphology.

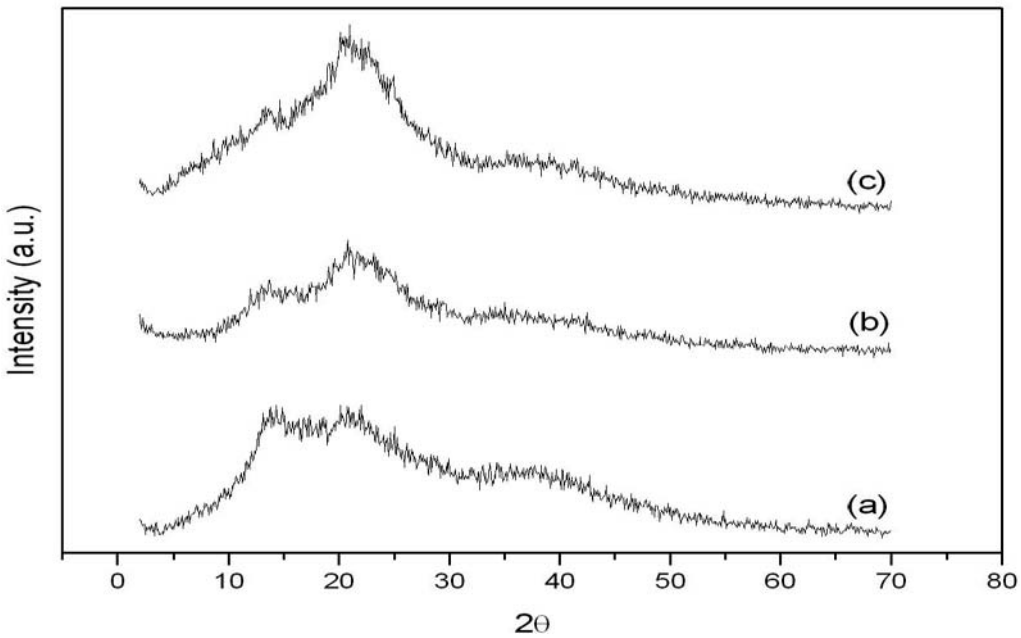

Figure 7.4 X-ray diffraction patterns, Alginic Acid (a), ALTri$_{0.5}$ (b), and ALTri$_{1.5}$ (c)

7.3 THERMAL ANALYSIS

7.3.1 Thermogravimetric Analysis (TG)

Thermogravimetric analysis has become an indispensable analytical technique for materials characterization. It involves continuous weighing of the polymer as it is

subjected to a temperature program and provides quantitative and qualitative kinetic information on the degradation, oxidation, evaporation or sublimation of material under investigation (Craver, 1983). Thermogravimetric analysis is also important for compositional analysis and determination of the additives in particular. The determination of the moisture content in polymer is also possible (Wundelich, 1990, Brennan, 1977).

7.3.1.1 TG of PAMPSATri$_x$

The thermal stability of the PAMPSATri$_x$ (x = 1, x = 2) electrolytes was studied by thermogravimetric analysis (TG) and PAMPSATri$_x$ shows a better thermal stability as illustrated in Fig. 7.5. These polymer electrolytes show 5-8 % weight loss between 130 and 220 ^{o}C under nitrogen atmosphere. They decompose in a single step above 220 ^{o}C, which is attributed to loss of sulfonic acid groups, then followed by the degradation of polymer backbone (Erdemi et al., 2004).

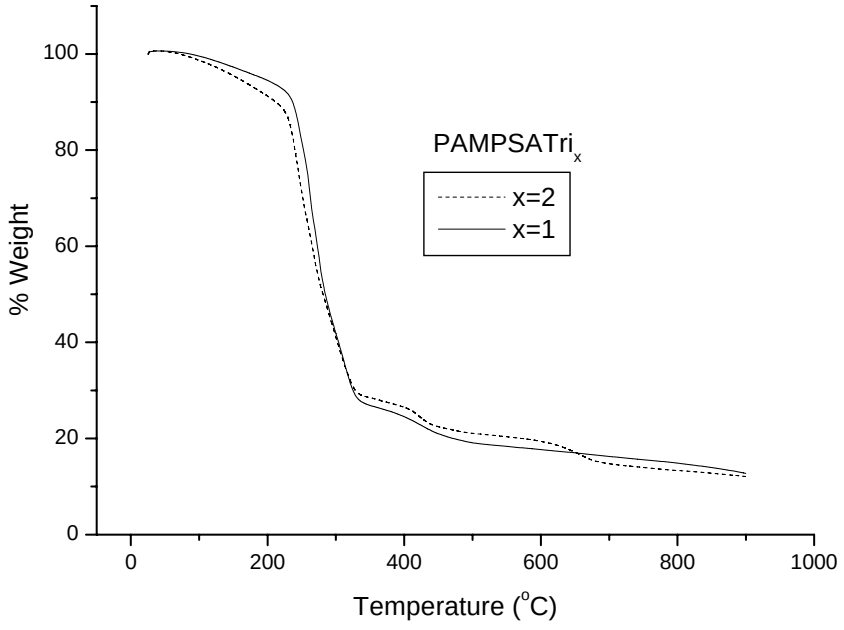

Figure 7.5 TG profiles of PAMPSATri$_x$ electrolytes. Heating rate is 10 ^{o}C/min under nitrogen.

7.3.1.2 TG of PVPATri$_x$

The thermal stability of the PVPATri$_x$ (x=1, x=1.5) electrolytes was studied by thermogravimetric analysis (TG) and depicted in Figure 7.6. PVPATri$_x$ electrolytes exhibited a thermal stability up to 150 ^oC then they decompose.

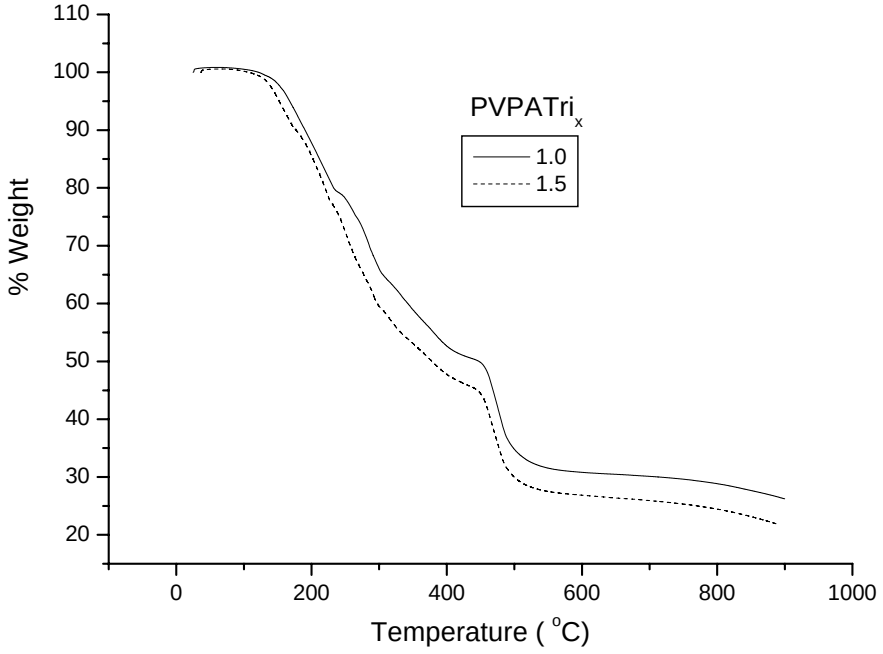

Figure 7.6 TG profiles of PVPATri$_x$ electrolytes. Heating rate is 10 ^oC/min under nitrogen atmosphere.

7.3.1.3 TG of ALTri$_x$

Figure 7.7 shows the TG thermograms of AL, ALTri$_{0.5}$, ALTri$_1$ and ALTri$_{1,5}$ from room temperature to 600 ^oC at a heating rate of 10 ^oC/min. Alginic acid shows initially dehydration process followed a one step decomposition above 185 ^oC. ALTri$_{0.5}$ shows no weight change up to 155 ^oC then it decomposes. Similarly, the onset of decomposition of both ALTri$_1$ and ALTri$_{1.5}$ is approximately 150 ^oC.

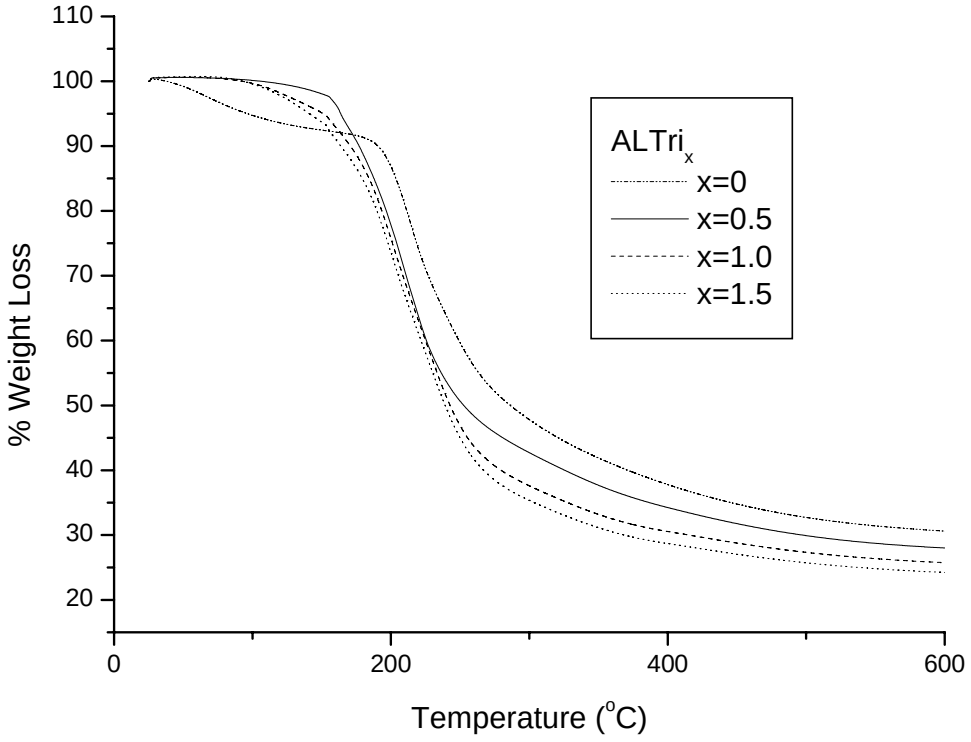

Figure 7.7 TG Curves of Alginic Acid and $ALTri_x$ Electrolytes. Heating rate is 10 ^oC/min under nitrogen atmosphere.

7.4 DIFFERENTIAL SCANNING CALORIMETRY (DSC)

Differential Scanning Calorimetry is most widely used methods of the thermal analysis in polymer science. They monitor the heat exchange can be physical or chemical in the nature. Polymerization or structural changes are almost invariably accompanied by energetic effects. E.g. crystallization, melting, curing and other reactions, and glass transition all show characteristic DSC curves. In the DSC, small samples (a few mg) are used and rapid heating (+q), rates up to 50-100 K/min are common. This technique is of great value for carrying out kinetic studies. Even if there are some similarities in equipment and application, DSC and DTA are different in their measurement system. In DTA, the sample and reference are heated by a single heat source with the same rate. The temperature difference between sample and reference ($\Delta T=T_s-T_r$) is measured and plotted as a function of sample temperature (T_s).The deviation of the sample temperature, T_s from T_r (ΔT) is directly proportional to the heat capacity. In DSC, the sample and reference are provided with different heaters and both

sample and reference cells are kept at the same programmed temperature (T_p). The temperature of each cell is measured continuously and compared with the instantaneous value of T_p. When a sample undergoes a thermal transition, the power to the two heaters is adjusted to maintain T_p and signal proportional to the power difference is plotted versus T_p. The power difference is $W_s (T_s-T_p) - W_r (T_r-T_p)$, where the first term is the power delivered to the sample and second is power delivered to the reference (Crompton, 1989, Compbell and White, 1989).

7.4.1 Glass Transition Temperature (Tg)

Glass transition phenomenon manifests a transition from a glassy amorphous polymer to a flexible material on warming through Tg. At this temperature the variables entropy, S, volume, V, enthalpy, H, merely change slope with increasing temperature. Large scale segmental motions of the polymer chain occur above this temperature. The location of Tg depends on the rate at which the temperature variation is carried out.

7.4.2 Variation of Glass Transition Temperatures

The T_g lowering phenomenon which can occur when a nonpolymeric liquid is incorporated into some polymers is known as plasticization. The addition of nonvolatile dioctylphtalate politicizes poly(vinyl chloride) and provides a shifting of glass transition below ambient temperature (Compbell, 1994).

Plasticization may be explained by a simple model shown in Figure 7.8. The three polymer chains are close to each other as represented in the diagram by irregular lines (a). This structural feature hinders the rotation of segments of the molecular chain and increases the distance between chains, allowing chain segments to move into the space which they occupy before the liquid ‘flows’ into the volume from which the chain segment moves (b). The corresponding situation within the polymer is that less thermal energy in total is required to keep the segmental motion going and consequently it undergoes the transition into the glassy state at a lower Tg after plasticizer has been added.

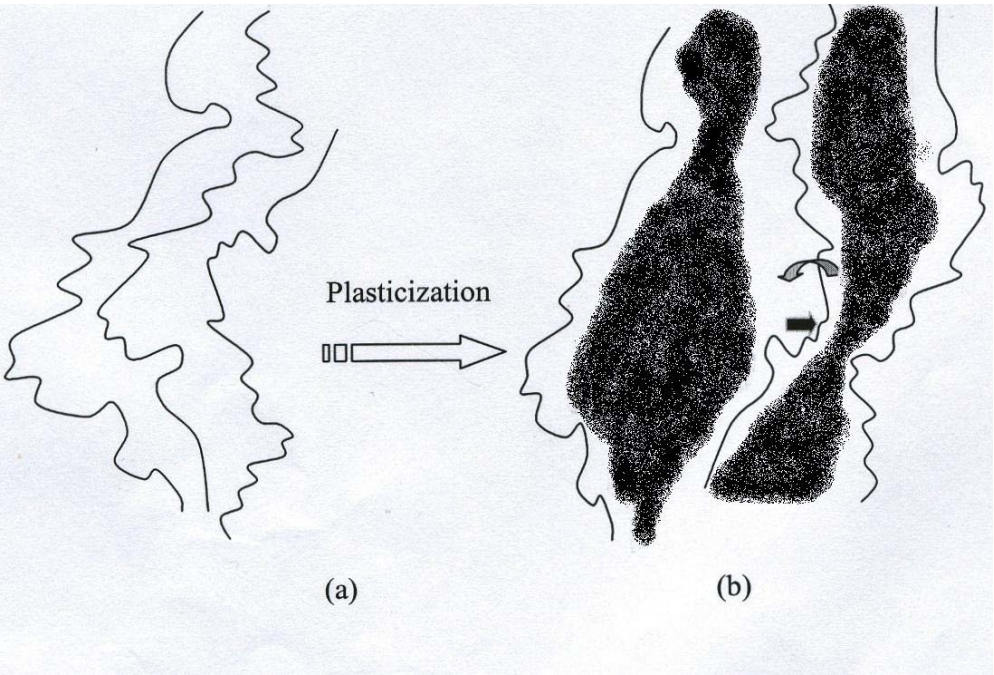

Figure 7.8 Plasticization with low molecular weight compound (Compbell, 1994)

7.4.3 DSC Studies of PAMPSA and PAMPSATri$_x$

PAMPSATri$_x$ membranes show no evidence of crystallization or melting point in DSC measurements which proves that it is amorphous. Figure 7.9 shows the DSC thermograms of the PAMPSATri$_x$ electrolytes. The T_g of the homopolymer, PAMPSA is 108 ^oC. PAMPSATri$_{0.5}$ gave lower T_g (39 ^oC) than PAMPSA, in the case of PAMPSATri$_1$ the T_g is 14 ^oC which is lower compared to x=0.5. The introduction of 2 triazole for each repeating unit resulted in the lowest T_g (-13 ^oC) in contrast to other compositions. From these results it can be concluded that the addition of Tri into PAMPSA plasticized the pristine polymer by shifting the T_g to lower temperatures.

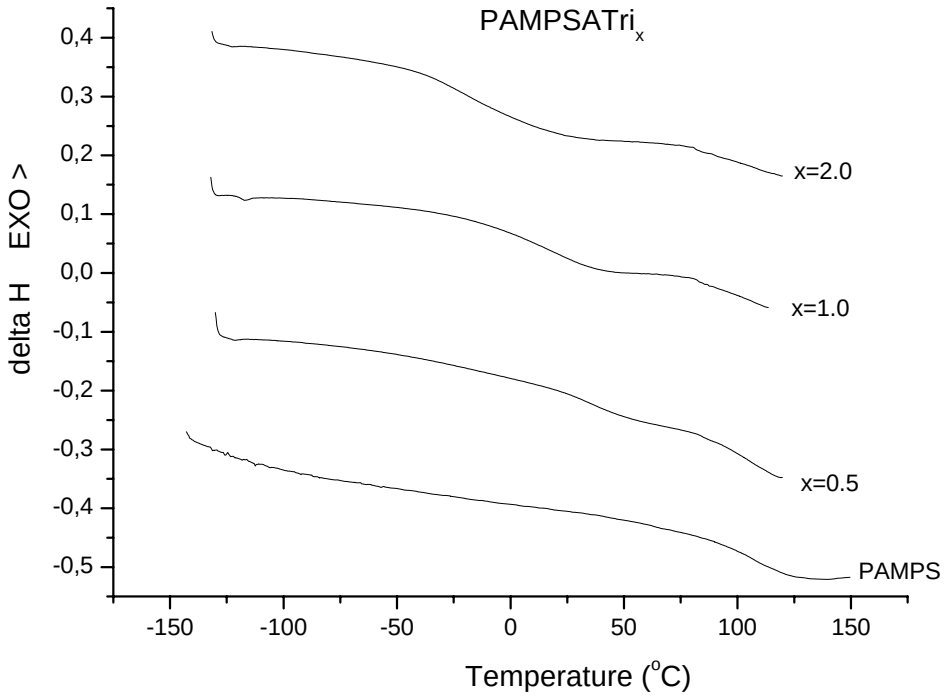

Figure 7.9 DSC thermograms of PAMPSATri$_x$ electrolytes under a N_2 atmosphere at a heating rate of 10 ^{o}C/min.

7.4.4 DSC Studies of PVPA and PVPATri$_x$

PVPATri$_x$ membranes show no evidence of crystallization or melting point in DSC measurements which proves that they are amorphous. DSC thermograms of PVPA and PVPATri$_x$ (x = 1 and x = 1.5) are presented in Fig. 7.10. PVPA has glass transition temperature, T_g of -23 ^{o}C. The addition of triazole (x=1) slightly increases the T_g of the blend to -15 ^{o}C. This can be attributed to complexation through formation of ionic groups which may restrict the segmental mobility of the polymer chains. When x = 1.5 the material softens and the T_g of the blend shifts to -20 ^{o}C.

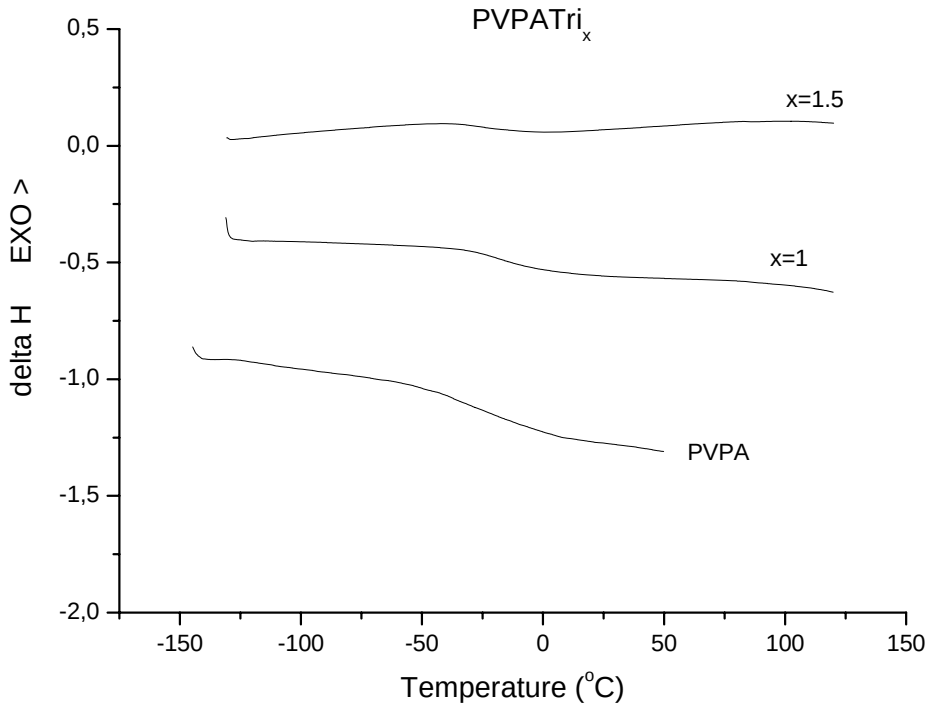

Figure 7.10 Comparison of the DSC thermograms of $PVPATri_x$ electrolytes under a N_2 atmosphere at a heating rate of 10 ^oC/min.

7.4.5 DSC Studies of AL and $ALTri_x$

Differential scanning calorimetry (DSC) was employed to determine thermal transitions in the complex electrolytes. The measurements were carried out from -100 ^oC to decomposition temperature of the complex electrolytes under nitrogen atmosphere and at a heating rate of 10 ^oC/min. DSC results demonstrated no glass transitions up to onset of the degradation. The reason of such a behavior can be attributed to restriction of segmental relaxation of the host polymer through complexation (Bozkurt et al., 2003).

7.5 CONDUCTIVITY OF POLYMER ELECTROLYTES

The ion conductivity in some inorganic crystals such as α- AgI, $Rb_4Cu_{11}I_7C_{13}$, ß-Alumina and Nasicon reaches values between 10^{-3}-10^0 S/cm at ambient temperature

(Takahashi, 1989, Laskar and Chandra, 1989).The mixtures of polymers with alkali metal salts have been extensively studied in the last few decades (Armand, 1983, Cowie and Sadaghianizadeh, 1990).The study of PEO/inorganic salts mixtures started from the analysis of the structure of a solid crystalline complex and it was proposed that helical PEO surrounds the cation which interacts with the lone electron pairs of the oxygen atoms. Ionenes are polyelectrolytes with N^{+}- cations as a part of their polymer repeat unit, with low molecular weight anions to balance the columbic charges. They have been analyzed by several groups (Dominiquez and Meyer, 1988, Rietz et al., 1994). In addition to these, poly-p-phenylene sulfonate and polystyrene sulfonate are also conductive, however, only one type of ion is mobile ("single ion conductors"). These single ion conducting polyelectrolytes have ionic groups such as $–SO_3^-$, $-CO_2^-$.They conduct by the counter cations. Generally the ionic conductivities of these single ion conducting polymers are 10^{-2} that of the ordinary amorphous ion–conductive polymers because of low ionization sulfonate or carboxylate salts in comparison with $MClO_4$ or MCF_3SO_3 (M=metal ion) inorganic compounds.

Recently, a similar strategy as in polymer /salt mixtures was followed by the polymer-inorganic acid complexes in order to achieve the required proton conductivity (Przyluski and Wieczorek, 1991).The above mentioned "polymer electrolytes" and "polyelectrolytes" are known to conduct the electricity by the transport of free ions. The electrical conductivity measurements of these materials are performed with both, direct current (DC) and alternating current (AC) measurements. The former method is accomplished by sandwiching the material between two nonblocking or blocking electrodes and a DC voltage is applied. Then from the resulting current, the resistance of the sample is measured (Linford, 1990). The latter method, AC measurements, is the most popular approach for the determination of electrical properties of polymer electrolytes. In this method a sinusoidal voltage is applied to a cell which functions as a capacitor and the resulting impedance is determined. The details of the conductivity measurements by an ac experiment will be explained in the following sections.

7.5.1 AC Conductivity Measurements

The measurement of the ionic conductivity with AC impedance spectroscopy has become a standard method simply because it is possible to separate the impedance

contribution form the relaxation processes and eliminate the effect of the electrode polarization. The measurements are carried out within the frequency range 10^{-2} –10^{7} Hz. The sample is sandwiched between two blocking electrodes, and a sinusoidal voltage is applied to the cell (Figure 7.11).

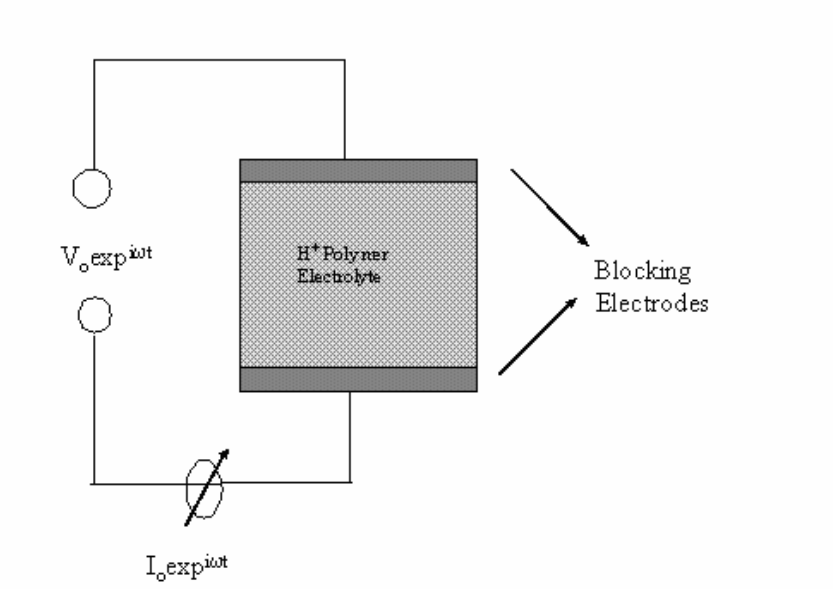

Figure 7.11 Circuit for AC impedance measurements (Blythe, 1979)

When an ac voltage is applied the frequency dependent complex dielectric constant ε^* presented by (eq. 7.1) (Blythe, 1979)

$$\varepsilon^* = \varepsilon' - i\,\varepsilon'' = \frac{C^*}{C_o} \qquad \textbf{(7.1)}$$

where C_o (eq. 7.2) is the capacitance between plates in the absence of the sample.

$$C_o = \varepsilon_o \frac{A}{d} \qquad \textbf{(7.2)}$$

and ε_o is the vacuum permittivity (ε_o = 8.852x10^{-14} F/cm), A, and d are the area and distance between the plates respectively. The C^* is the complex capacitance with the sample. The frequency dependent voltage V (t), and current I (t) are given by (eq. 7.3);

$$I(t) = \frac{dq(t)}{dt} = \frac{d[\ C^*\ V(t)\ ]}{dt} = i\omega C_o\, \varepsilon^*\, V(t) \qquad \textbf{(7.3)}$$

from the equations (7.2) ,(7.3) and the (7.4) is obtained

$$\frac{I(t)}{V(t)} = \frac{1}{Z^*(t)} = \omega C_o\ (\ \varepsilon'' + i\ \varepsilon\ ) \qquad \textbf{(7.4)}$$

It is convenient to consider the sample as being frequency dependent capacitance, C_p and the resistance, R_p in a electrically equivalent parallel circuit. The complex impedance is Z* (t) given as

$$\frac{1}{Z^*(t)} = \frac{1}{R_p} + i\omega C_p \qquad \textbf{(7.5)}$$

and comparing the equations (7.4) and (7.5) the real and imaginary parts of ε* are obtained with parallel capacitor, C_p and R_p parallel resistor

$$\varepsilon' = \frac{C_p}{C_o} \qquad \textbf{(7.6)}$$

$$\varepsilon'' = \frac{1}{R_p\, \omega\, C_o} \qquad \textbf{(7.7)}$$

the loss factor (eq. 7.8) which is related with the heat loss in the material due to the motions of the charges and dipoles is;

$$\tan \delta = \frac{\varepsilon''}{\varepsilon'} \tag{7.8}$$

and the complex conductivity is σ* (eq. 7.9)

$$\sigma^* = \sigma' + i\,\sigma'' = i\omega\,\varepsilon_o\,\varepsilon^* \tag{7.9}$$

the frequency dependent AC conductivity, σ_{ac} is defined by (eq. 7.10) and (eq. 7.11)

$$\sigma(\omega) = \mathrm{Re}\,\sigma^*(\omega) \tag{7.10}$$

$$\sigma_{ac}(\omega) = \sigma'(\omega) = \varepsilon''(\omega)\,\omega\,\varepsilon_o \tag{7.11}$$

7.5.2 DC Conductivity Measurements

The determination of the DC conductivity from ε" versus log frequency data was explained by Havriliak-Negami fit equation. The conductivity region is separated from the relaxation part and the corresponding ionic conductivity is obtained. Generally the observation of plateaus at low frequencies of log σ_{ac} against log F (frequency independent values of conductivity) corresponds to DC conductivity, σ_{dc}. σ' can be written (eq. 7.12) (Chen et al., 1992, Chowdari and Gopalakrishnan, 1987).

$$\sigma' = \sigma(0) + \sigma(0) \quad \frac{\omega^p}{\omega_s^p} \tag{7.12}$$

σ (0) represents the DC conductivity when frequency is extrapolated to zero (eq. 7.13)

$$\lim_{\omega \to 0} \sigma'(\omega) \to \sigma_{dc} \tag{7.13}$$

and ω_s is the critical frequency at which dispersion of conductivity begins and p represents the slope of the dispersion region at higher frequencies and it is related to the carrier hopping rate. The conductivity at ω_s is given by (eq. 7.14)

$$\sigma(\omega_s) = 2\sigma(0) \tag{7.14}$$

7.5.3 Theoretical Treatment of Ion Conduction in Solid Electrolytes

Ionic compounds and polymers can be categorized according to their conductivity: (i) *insulators* with ionic conductivity lower than 10^{-10} S/cm, (the electronic contribution to the conductivity is in the same range). (ii) *ionic conductors*; the presence of charge carries increases the conductivity up to 10^{-5} S/cm. (iii) *superionic conductors* with conductivity of at least 10^{-4} S/cm.

7.5.3.1 Ion Conduction in Solid Electrolytes

The bulk conductivity in solid electrolytes depends on the concentration of free ions (eq. 7.15) (Reisinger, 1998). The concentrations of these charge carries and their motilities should be high since;

$$\sigma = \sum n_i (z_i e) \mu_i \qquad \textbf{(7.15)}$$

n_i is the number of carries of type i, $z_i e$ is the net electronic charge on the ion or aggregate, and μ_i is mobility. The energies of activation of the formation and diffusion of these charge carries should be higher than that of potential barriers to transport the ions. The ionic mobility, μ_i is related to the diffusion coefficient D_i by the Nerst – Einstein (NE) equation (eq. 7.16)

$$\mu = \frac{z_i e D_i}{kT} \qquad \textbf{(7.16)}$$

this yields with (eq. 7.15) the conductivity (eq. 7.17)

$$\sigma = \frac{n_i (z_i e)^2 D}{kT} \qquad \textbf{(7.17)}$$

The conductivity in the glassy state may sometimes be expressed by the Arrhenius equation (eq. 7.18)

$$\sigma = \sigma_o \exp(-E_a / kT) \qquad \textbf{(7.18)}$$

E_a is activation energy for conductivity and σ_o is the pre exponential factor.

7.5.3.2 Ion Conduction in Amorphous Polyelectrolytes

The multiphase behavior in a material influences the ion conductivity since the presence of both, crystalline and amorphous regions introduce phase boundary effects. The ion conductivity is usually higher in the amorphous region. The conductivity of the crystalline material increases rapidly when it melts. In order to understand the ionic motion in solid electrolytes, fully homogeneous amorphous polymer-salts or polyelectrolytes are considered. In this type of conductor the ion transport strongly

depends on the ion diffusion, which is cooperative rearrangement of the polymer segments, i.e., associated with a local free volume or viscosity of the material. The temperature (and frequency) dependent viscosity of amorphous polymers can be described by the Vogel-Tammann-Fulcher, VTF equation (eq. 7.19) (Ratner, 1987)

$$\eta = C \exp\left(\frac{-B}{k(T-T_o)}\right) \text{ with } C \alpha T^{1/2} \qquad \textbf{(7.19)}$$

The empirical relationship (Doolittle eq.) (eq. 7.20) between viscosity and free volume of the material can be represented by the formula 7.20.

$$\eta = A \exp(b_o \upsilon_o / \upsilon_f) \qquad \textbf{(7.20)}$$

b_o is a dimensionless constant, υ_o is the van der waals volume and υ_f is the average free volume. From the Stokes Einstein relation (Gauthier et al., 1988) the VTF conductivity eqution (7.21) results

$$\sigma = \sigma_o \exp\left(\frac{-B}{k(T-T_o)}\right) \qquad \textbf{(7.21)}$$

where T_o is the Vogel temperature generally placed ~ 50K below the glass transition temperature which is idealized as the temperature at which all “free volume” vanishes or all polymer segmental motions disappear or the configurational entropy of the material vanishes. The σ_o contains a $T^{-1/2}$ term and some other constants, B is proportional to a characteristic hard sphere volume of the moving polymer chain segment or to the inverse expansivity of the material. This equation shows the conductivity and viscosity relation as a function of temperature. The WLF (eq. 7.22) equation includes both the viscosity and relaxation processes in amorphous systems.

$$\sigma = \sigma(T_r)\exp\left(\frac{C_1[T - T_r]}{C_2 + T - T_r}\right) \quad \textbf{(7.22)}$$

where C_1 and C_2 are constant which are obtained experimentally , T_r is a reference temperature.

Both WLF and VTF equations are identical when; $C_1C_2 = B$ and $C_2 = T_r - T_o$. These two equations offer several advantages: they describe the temperature dependent conductivity and transport properties including, viscosity and conductivity. They allow for an interpretation of several parameters such as T_o (VTF temperature) and V_f (free volume).

However, they don't give information about the microscopic structure such as molecular weight dependence of the ion transport and the mechanism of ion transport. To understand the microscopic transport the "Dynamic Bond Percolation" model was suggested for amorphous materials (Ratner, 1987). The static percolation model can be defined as the set of sides at which the moving ions can reside (hopping process).This is valid in the glassy framework of solid electrolytes. When the $T>T_g$, then the static bond percolation model can not characterize the ion motion, in this case the motion of ions occurs dynamically by means of coordinated segmental motions of the polymer host timescales.

7.5.4 Proton Conductivity in Blends of PAMPSATrix and PVPATri$_x$

The conductivities of PAMPSATri$_{x,}$ and PVPATri$_x$ materials were measured within the frequency range of 0.1 Hz to 10 MHz and temperature range of 20-140^{o}C for PAMPSATri$_x$ and -20-120 ^{o}C for PVPATri$_{x.}$

The thin films of PAMPSATri$_x$ and PVPATri$_x$ samples were sandwiched between two platinum electrodes by heating them above their glass transition temperatures. AC conductivities were obtained using $\sigma_{ac} = \varepsilon''(\omega)\ \omega\ \varepsilon_o$ where ε_o is the vacuum permittivity, ω is angular frequency and $\varepsilon''(\omega)$ is the loss factor. AC conductivity versus frequency

plots (in a log scale) were displayed in Fig. 7.12 for $PAMPSATri_2$ and Fig. 7.13 for $PVPATri_{1.5}$.

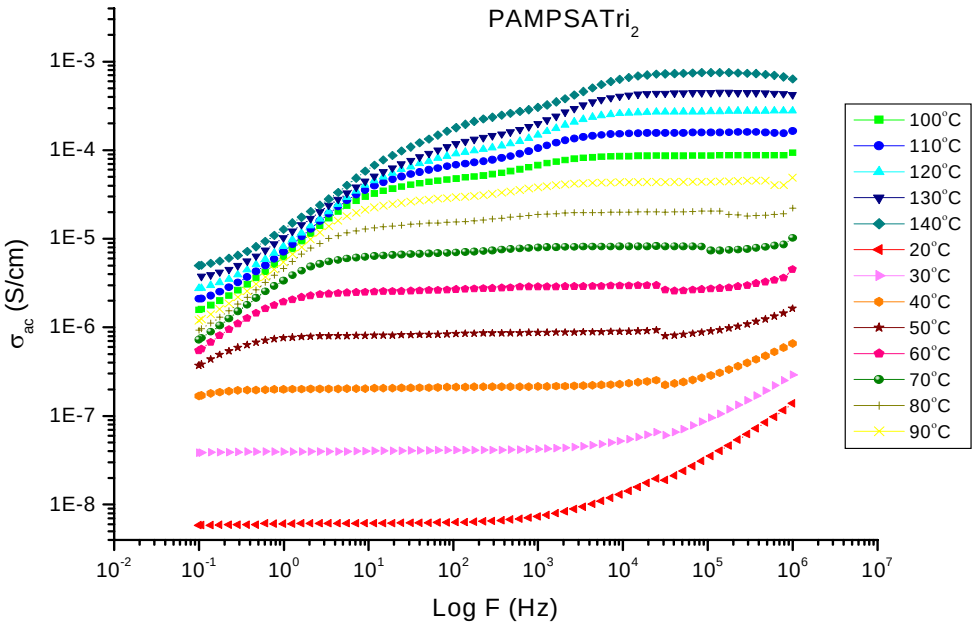

Figure 7.12 AC conductivity vs. frequency of $PAMPSATri_2$ at several temperatures.

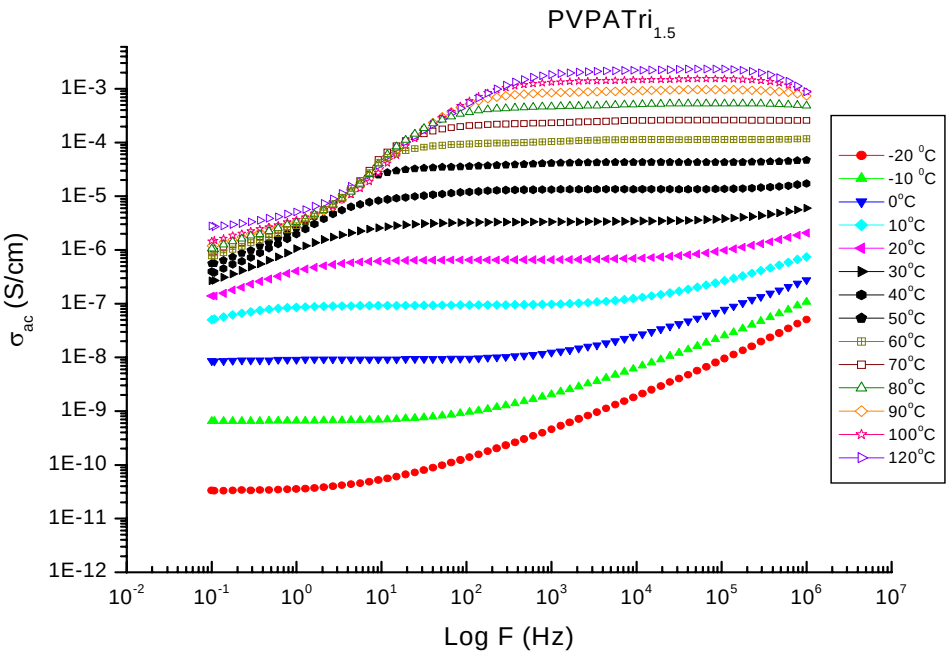

Figure 7.13 AC conductivity vs. frequency of $PVPATri_{1.5}$ at several temperatures.

Generally, for ion conducting electrolytes log σ_{ac} vs. log F comprise several regions (Rietz and Meyer, 1993, Rietz et al., 1994) at lower temperatures, frequency independent conductivity plateaus (over 1 to 4 decades) corresponding to the DC conductivity which shift to higher frequencies at higher temperatures. At higher temperatures, the irregularities at the low frequency side correspond to polarization of the blocking electrode-electrolyte interface and conductivity increase at low temperature and high frequency region belongs to normal dispersion in polymer electrolytes. The DC conductivities of these samples were obtained by linear fitting the plateau values to real axis. The corresponding σ_{dc} conductivities obtained by this method coincide well with the one that evaluated from the Nyquist plot, so that the values extrapolated from σ_{ac} plateaus to be good estimation (Kufacı et al., 2006)

The data which show the temperature dependence of proton conductivity of the $PVPATri_x$ and $PAMPSATri_x$ membranes are presented in Fig. 7.14. It was demonstrated that the proton conductivities of the anhydrous materials increase with increasing temperature. There is no contribution of segmental relaxations to the proton conductivity of $PVPATri_{1.5}$ below the temperature (3.7) shown in Fig. 7.14. That is why conductivity data of $PVPATri_{1.5}$ deviated from the VTF curve.

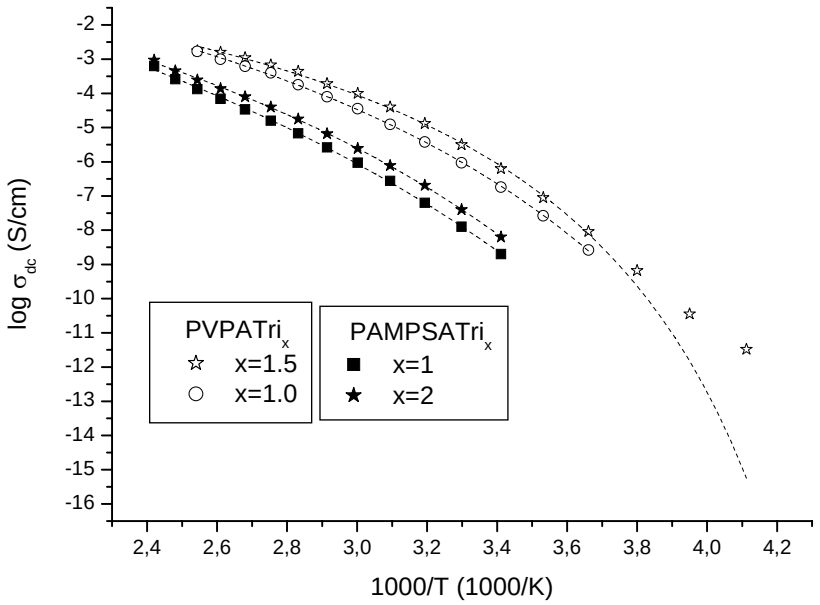

Figure 7.14 Anhydrous proton conductivity versus reciprocal temperature for $PVPATri_1$, $PVPATri_{1.5}$, $PAMPSATri_1$, and $PAMPSATri_2$ electrolytes. Dash lines illustrate the VTF fits.

The Arrhenius plots show curvilinear lines irrespective of type of host polymer and triazole concentration. They can be interpreted by Vogel-Tamman-Fulcher, VTF relationship, Eq. 7.23.

$$\log \sigma = \log \sigma_o - \frac{E_v}{R\,(T-T_o)} \qquad \textbf{(7.23)}$$

At infinite T, R is gas constant, E_v and T_o are empirical parameters corresponding to Vogel activation energy and Vogel temperature (Pennarun and Jannasch, 2005). The conductivity isotherms were fitted with VTF equation and the results are illustrated in Table 7.1.

Table 7.1 Glass transition temperature (T_g), maximum conductivity and VTF parameters for $PVPATri_x$ and $PAMPSATri_x$ blends

Polymer-Triazole Blends	T_g (^oC)	Max. Conductivity (S/cm)	Log σ_o	T_o (K)	E_v (eV)
$PAMPSATri_1$	14	$6.3x10^{-4}$ at 140^oC	2.60	160	0.30
$PAMPSATri_2$	-13	$9.3x10^{-4}$ at $140\ ^oC$	1.20	180	0.22
$PVPATri_{1.5}$	-20	$2.3x10^{-3}$ at $120\ ^oC$	0.38	208	0.11
$PVPATri_1$	-15	$1.7x10^{-3}$ at $120\ ^oC$	1.48	187	0.17

The contribution of polymer segmental relaxation to proton conductivity is proved by the high accuracy of the VTF fits over a broad temperature range of 20-140^{o}C for $PAMPSATri_x$ and range of 0-120 ^{o}C for $PVPATri_x$. As shown in Table 7.1, the log σ_o values are ranging from 0.38 to 2.6 which shows the efficiency of triazole as proton

solvent in acidic polymer hosts. The difference between glass transition temperature and Vogel temperature (T_g-T_o) was found to be between 45 and 127 K.

Clearly, the proton conductivity of the anhydrous PVPA-Tri electrolytes is at least one order of magnitude higher than that of PAMPSA-Tri electrolytes. Even the electrolyte, $PVPATri_x$ with x = 1.5 has better conductivity than $PAMPSATri_x$ with x = 2. This behavior can be attributed to the polymer-Tri interactions not to the nature of the host matrix. It was also demonstrated that both PAMPSA and PVPA which contain 2 moles of imidazole (Im) per mole of polymer repeat unit (doping ratio), have almost identical proton conductivities (Erdemi et al., 2004, Sevil and Bozkurt, 2004). However, when the doping ratio was reduced to 1 then the maximum conductivity of PAMPSA-Im system was reported to be three orders of magnitude lower than that of PVPA-Im blends. Such a deviation was ascribed to the degree of protonation of the heterocyclic ring which was more pronounced in the PAMPSA-Im system.

As seen, the conductivity of $PVPATri_x$ electrolytes increases when x varies from 1 to 1.5 in the temperature range studied. Similar behavior was observed for $PAMPSATri_x$ electrolytes where x changed from 1 to 2. This can be explained by the increase in the unprotonated nitrogen sites as in the case of imidazole. Previously, the proton conduction in imidazole was proposed as the transfer of protons between neighboring protonated and unprotonated guest molecules through 'hop-turn' mechanism (Münch et al., 2001, Sevil and Bozkurt, 2004, Yamada and Honma, 2005). In that respect, a proton conductive pathway is constructed by the aggregation of imidazole moieties in hydrogen-bonded chains. The addition of Tri to acidic polyelectrolytes such as PVPA and PAMPSA resulted in the protonation of the heterocyclic ring as confirmed by FT-IR spectra of the electrolytes. High proton conduction occurs for both $PVPATri_1$ and $PAMPSATri_1$ implying the partial protonation of the heterocyclic rings. Therefore, proton conduction in $PVPATri_x$ and $PAMPSATri_x$ polymer electrolytes can occur through mobility of protonic defects via structure diffusion as in the case of polymer-imidazole systems (Grotthuss mechanism) (Fig. 7.15).

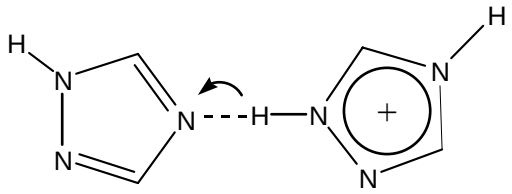

Figure 7.15 Intermolecular proton transfer mechanism between neighboring protonated and unprotonated triazoles.

Moreover, they may also aggregate to form dynamical hydrogen bonded chains, supporting long range high proton transport. The proton conductivity of liquid imidazole was reported to be approximately 10^{-3} S/cm at its melting point (90 ^{o}C) (Kreuer et al., 1998). Similarly the proton conductivity of 1,2,4-triazole reached to $1.2x10^{-3}$ S/cm in the molten state (Li et al., 2005). These new polymer electrolyte membranes show a maximum anhydrous proton conductivity of $2.3x10^{-3}$ S/cm for $PVPATri_{1.5}$ at 120 ^{o}C and of $9.3x10^{-4}$ S/cm for $PAMPSATri_2$ at 140 ^{o}C.

7.5.5 Proton Conductivity in Blends of $ALTri_x$

The AC conductivity data of $ALTri_x$ electrolytes were measured using an impedance spectroscopy within the frequency rage 1Hz to 1MHz. The samples were placed between gold electrodes and the complex conductivities were obtained at 10 ^{o}C interval under nitrogen atmosphere. Figure 7.16 shows the AC conductivity (σ_{ac}) of $ALTri_{1.5}$ versus frequency in a logarithmic scale. The curve comprises several regions depending on the temperature and frequency which are similar to other ion conducting polymers (Erdemi et al, 2004). Frequency independent conductivity regions which are formed at lower temperatures (T = 0-30 ^{o}C) shifts to higher frequencies at higher temperatures.

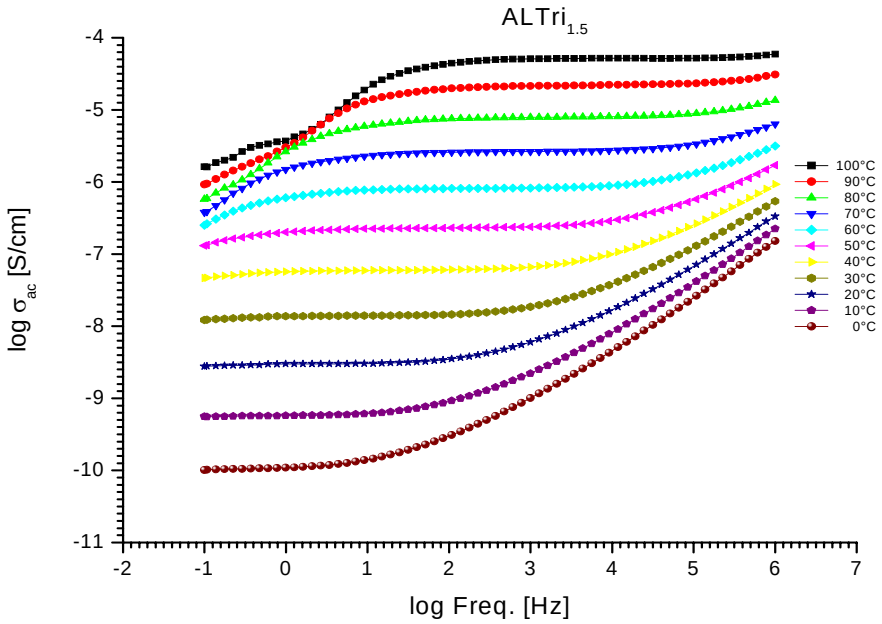

Figure 7.16 AC conductivity vs. log F (Hz) of $ALTri_{1.5}$ at various temperatures.

Moreover, normal dispersions in polymers can be observed at lower temperatures and higher frequencies, i.e., the conductivity increases sharply at T = 20 ^{o}C and the frequency higher than 100 Hz. When T > 50 ^{o}C, the irregularities at the low frequency side corresponds to electrode polarization. The DC conductivity (σ_{dc}) of the polymer electrolytes can be derived from the conductivity plateaus through linear fitting and extrapolating to the real axis.

The proton conductivities of the complex electrolytes were evaluated through heating and cooling cycles from 0 ^{o}C to 100 ^{o}C at 10 ^{o}C intervals. Arrhenius plots of the complex electrolytes with different concentrations of triazole are presented in Fig. 7.17.

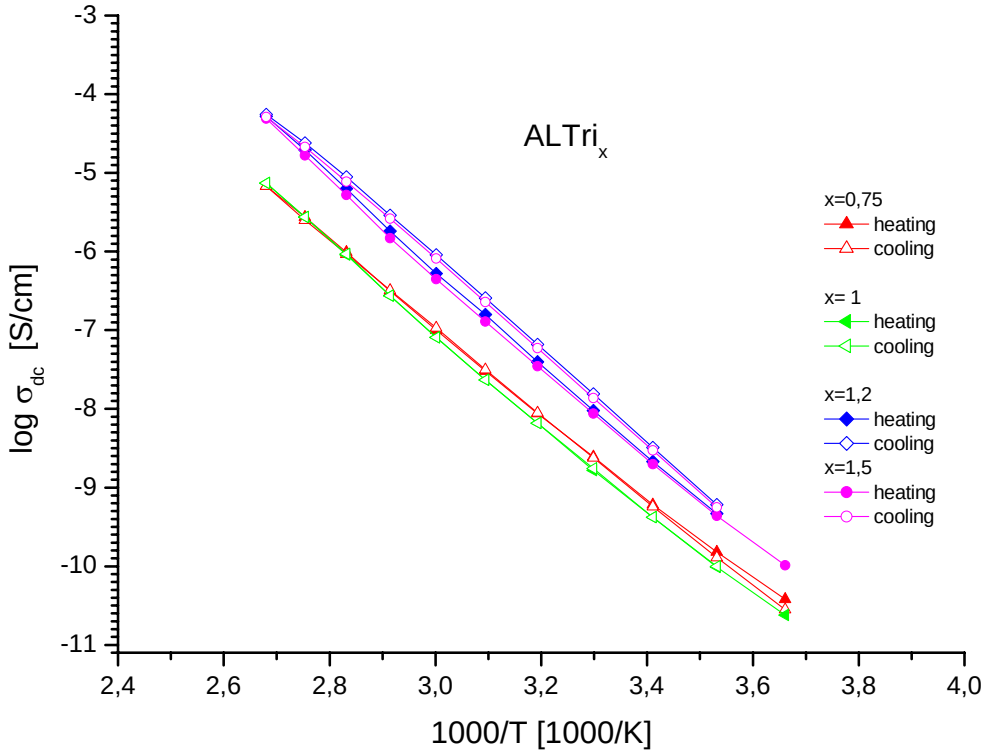

Figure 7.17 Proton conductivity versus reciprocal temperature of the complex electrolytes, ALTri$_x$.

The conductivities which are measured through heating or cooling are almost identical at the respective temperatures. This result shows the reproducibility of the proton conductivity when the samples have experienced temperatures up to 100 ^{o}C. The conductivity vs. reciprocal temperature shows straight lines which indicate the absence of cooperative segmental relaxations as proved by DSC. The data suggested that the conduction mechanism can be described by the simple Arrhenius equation (Eq. 7.24).

$$\sigma = \sigma_o \exp\left(-\frac{E_a}{kT}\right) \qquad \textbf{(7.24)}$$

where σ_o is the pre-exponential factor, k is the Boltzmann constant. E_a is the activation energy which can be estimated form the slope of the conductivity isotherms, Fig. 7.17.

The E_a values were very close to each other and found to be $1x10^{-3}$ - $1.2x10^{-3}$ eV (Table 7.2).

Table 7.2 Pre-exponential factor, log σ_o and the activation energy, E_a of $ALTri_x$ electrolytes

$ALTri_x$	**log σ_o**	**E_a (eV)**
$ALTri_{0.75}$	9.3	$1.1x10^{-3}$
$ALTri_1$	9.9	$1.13x10^{-3}$
$ALTri_{1.2}$	11.6	$1.2x10^{-3}$
$ALTri_{1.5}$	11.3	$1.2x10^{-3}$

These values are at least two orders of magnitude lower than other non-aqueous systems such as polymer-imidazole composite electrolytes (Yamada and Honma, 2005) and organic electrolytes (Yamada and Honma, 2004). These results suggested that rapid proton transfer occurs between triazole units. It was previously reported that heterocyclic molecules such as imidazole contain two nitrogen atoms and allow proton transfer from imidazolium ion to imidazole through structural reorientation (Münch et al., 2001). Triazole has a molecular structure similar to imidazole but it bears three nitrogen atoms in the ring. Intra- molecular proton transfer may occur by a process so called 'toutomerism' (Fig. 7.18) (Rauhut , 2003).

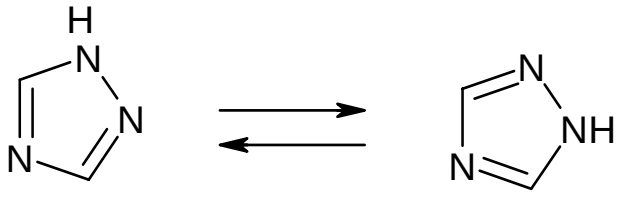

(a) (b)

Figure 7.18 Intra-molecular proton transfer via toutomerism, 1H-1,2,4-triazole (a) 2H-1,2,4-triazole (b)

Long range proton transfer may occur through intermolecular proton exchange reactions as in the case of imidazole (Münch et al., 2001). From the FT-IR studies we have confirmed the deprotonation of carboxylic acid group and protonation of the heterocyclic ring resulting in salt formation. Therefore proton transfer between triazolium ion and triazole can be the major pathway for the proton conduction and no translative motion of triazole rings. Similar conductivity mechanisms were also reported for 1,2,3-triazole (Zhou et al., 2005).

The proton conductivity of $ALTri_{0.75}$ and $ALTri_1$ are very close to each other within the temperature range of measurement. However, the conductivity increases at least one order of magnitude for $ALTri_{1.2}$ and $ALTri_{1.5.}$ The reason can be explained by the number of Tri per polymer repeat unit where up to x=1 all Tri is bound to ionic groups, while at x>1 the existence of free Tri can contribute to conductivity through structure diffusion. Maximum proton conductivity of the complex electrolytes was measured to be approximately 10^{-4} S/cm at 100 ^{o}C.

CHAPTER 8

CONCLUSIONS

In this work, 1,2,4-Triazole has been used as proton solvent in acidic polyelectrolytes. Several proton conducting polymer electrolytes were produced through blending of poly(vinylphosphonic acid), PVPA, and poly(2-acrylamido-2-methyl -1-propanesulfonic acid), PAMPSA to form $PVPATri_x$ and $PAMPSATri_x$.

The proton exchange reactions occur between polymer and Tri as illustrated by FT-IR data. $PVPATri_x$ and $PAMPSATri_x$ electrolytes exhibited a thermal stability up to 150 ^oC and 200 ^oC, respectively.

The homogeneity and amorphous morphology of the blends were found by DSC studies. Triazole acted as plasticizer in these polymer electrolytes.

The positive effect of the segmental relaxations on the proton conductivity was established by fitting the conductivity isotherms with VTF equation. The anhydrous proton conductivity of $PVPATri_x$ was higher than $PAMPSATri_x$ and exceeding 10^{-3} S/cm for the former at 120 ^oC. The proton migration may occur through intermolecular proton transfer reactions (Grotthuss mechanism).

As a separate work, Alginic acid, AL was employed as the host matrix and triazole was used as blend component. Transparent, homogeneous and thin films were obtained for all the systems. FT-IR studies proved the coexistence of both protonated and unprotonated triazole units. DSC results and conductivity isotherms proved the restriction of the segmental relaxations of the polymer through complexation. Maximum proton conductivity of ~ 10^{-4} S/cm was obtained for $ALTri_{1.5}$.

These polymer electrolytes have good film forming properties and can be suggested for application in high temperature PEM fuel cells as well as electrochromic devices and sensors.

REFERENCES

Acheson, R. M., *An Introduction to the Chemistry of Heterocyclic Compounds*, John Wiley, Canada, 1976.

Allcock, H. R., Hofmann, M. A., Ambler, C. M., "Phenyl phosphonic acid functionalized polywaryloxyphosphazenesx as proton-conducting membranes for direct methanol fuel Cells", *Journal of Membrane Science*, Vol. 201, pp. 47–54, 2002.

Appleby A. J., Foulkes F. R., *Fuel Cell Handbook*, Van Nostrand Reinhold, New York, 1989.

Armand, M., "Polymer solid electrolytes-An Overview", *Solid State Ionics*, Vol. 9&10, pp.745-754, 1983.

Asensio, J. A., Borro´s, S., Go´mez Romero, "Proton conducting polymers based on benzimidazole and sulfonated benzimidazoles", *Journal of Polymer science: PolymChem*. Vol. 40, pp. 3703–10, 2002.

Bae, J. M., Honma, I., Murata, M., Yamamoto, T., Rikukawa, M., Ogata, N., "Properties of selected sulfonated polymers as proton-conducting electrolytes for polymer electrolyte fuel cells", *Solid State Ionics*, Vol. 147, pp. 189–94, 2002.

Berzins, T., *Journal of Electrochemical Society*, Vol. 124(8), pp. C318, 1977.

Besse, S., Capron, P., Diat, O., "Sulfonated polyimides for fuel cell electrode membrane assemblies (EMA)", *Journal of New Material Electrochemical Systems*, Vol. 5, pp. 109–12, 2003.

Bloys van Treslong, C.J., Staverman, A.J., *Rec. Trav. Chim., Pay-Bas,* Vol. 93(6), pp. 171–178, 1974.

Blythe, A. R., *Electrical Properties of Polymers*, Cambridge University Pres, pp.38-71 Cambridge, 1979.

Bozkurt, A., Meyer, W. H., *Solid State Ionics*, Vol. 138, pp. 259–265, 2001.

Bozkurt, A., Meyer, W. H., Wegner, G., *Journal of Power Sources*, Vol. 123, pp. 126, 2003.

Brennan, W. P., *Thermochimica Acta*, Vol. 18 pp.101-111, 1977.

Buckley, A., Stuetz, D. E., Serad, G. A., *In Encyclopedia of Polymer Science and Engineering*, Second Edition, Vol. 11, pp. 572–601, New York, Wiley & Sons, 1988.

Carter, R., Wycisk, R., Yoo, H., Pintauro, P. N., *Electrochemica Solid State Letter*, Vol. 5, pp. A195–A197, 2002.

Chandra, S., Hashmi, S. A., Prasad, G., "Studies on Ammonuim Perchlorate Dopped Polyethylene Oxide Polymer Electrolyte", *Solid State Ionics*, Vol. 40-41, pp. 651-654, 1990.

Chen, R., Yang, R., Durand, B., Pradel, A., Ribes, M., *Solid State Ionics*, Vol. 53-56, pp.1194-1199, 1992.

Chin, D. T., Chang, H. H., *Journal of Applied Electrochemistry*, Vol. 19(1), pp. 95–99, 1989.

Chowdari, B. V. R., Gopalakrishnan, R., *Solid State Ionics*, Vol. 23, pp. 225-233, 1987.

Compbell, I. M., *Introduction to Synthetic Polymers*, Oxford University Press, 1994.

Compell, D., White,J. R., "Polymer Characterization", *Chapman & Hall*, NJ, 1989.

Cowie, J. M. G., Sadaghianizadeh, K., *Solid State Ionics*, Vol. 42, pp. 243, 1990.

Craver, C. D., "Polymer Characterization", *American Chemical Society*, Ch.12, 1983.

Crompton, T. R., *Analysis of Polymers*, Pergamon Pres, pp. 16, 1989.

Daniel, M.F., Desbat, B., Cruege, F., Trinquet, O., Lass`egues, J.C., *Solid State Ionics*, Vol. 28, pp. 637–41, 1988.

DesMarteau, D. D., *Journal of Fluorine Chem.*, Vol. 72, pp. 203, 1995.

Ding, J., Chuy, C., Holdcroft, S., *Adv Funct Mater.*, Vol. 12, pp. 389–94, 2002.

Dippel, T., Kreuer, K. D., Lass`egues, J. C., Rodriguez, D., *Solid State Ionics*, Vol. 61(1–3), pp. 41–46, 1993.

Dominiquez, L., Meyer, W. H., *Solid State Ionics*, Vol. 28-30, pp. 941-949, 1988.

Donoso, P., Gorecki, W., Berthier, C., Defendini, F., Poinsignon, C., Armand, MB., *Solid State Ionics*, Vol. 28, pp. 969–74, 1988.

Doyle, M., Wang, L., Yang, Z., Choi, S. K., *Journal of Electrochemical Society*, Vol. 150, pp.185, 2003.

Erdemi, H., Bozkurt, A., Meyer, W. H., *Synthetic Metals*, Vol. 143, pp. 133, 2004.

Fontanella, J. J., Wintersgill, M. C., Wainright, J. S., Savinell, R. F., Litt, M., *Electrochimica Acta,* Vol. 43(10–11), pp. 1289–94, 1998.

Fuell Cell Hand Book, Parsons Inc., West Virginia, 2000.

Genies, C., Mercier, R., Sillion, B., Cornet, N., Gebel, G., Pineri, M., *Polymer* ,Vol. 42 ,pp. 359–73, 2001.

Genies, C., Mercier, R., Sillion, B., *Polymer* ,Vol. 42, pp. 5097–105, 2001.

Gillham, J. K., *Macromolecule Science,* Vol. 1, pp. 83, 1972.

Glipa, X., Bonnet, B., Mula, B., Jones, D. J., Rozi`ere, J., *Journal of Material Chem.*, Vol. 9(12), pp. 3045–49, 1999.

Goldner, R. B., Haas, T. E., Seward, G., Wong, K. K., Norton, P., Foley, G., Berera, G., Wei, G., Schulz, S., and Chapman, R., *Solid State Ionics*, Volumes 28-30, Part 2, pp 1715-1721, 1988.

Goldner R. B., Arntz,F. O., Berera, G., Haas, T. E., Wei, G. K., Wong, K., and Yu, P. C., *Solid State Ionics*, Vol. 53-56, Part 1, pp. 617–627, 1992.

Granqvist, C. G., "Electrochromism and Smart Window Design", Solid State Ionics, Vol. 53-56, pp. 479-489, 1992.

Grot, W., To, E.I., Du Pont De Nemours and Company, U.S. 3,718,627, 1968.

Guathier Armand, M., Muller, D., Skotheim, T.A., Electroresponsive Molecular and Polymeric Systems, Merkel Dekker Inc., 1988.

Guo, X., Fang, J., Watari, T., Tanaka, K., Kita, H., Okamoto, K., *Macromolecules*, Vol. 35, pp. 6707–13, 2002.

Hickner, M. A., “Transport and Structure in Fuel Cell Proton Exchange Membranes”, 2003.

Hofmann, M. A., Ambler, C. M., Maher, A. E., *Macromolecules*, Vol. 35, pp. 6490–3, 2002.

Hogarth, M., Glipa, X., “High Temperature Membranes For Solid Polymer Fuel Cells”, ETSU F/02/00189/REP DTI/Pub URN 01/893 , 2001.

Hogdon, R. B., *Jornal of Polymer Science: Gen. Pap.*, Vol. 6, pp. 171, 1968.

Honma, I., Hirakawa, S., Yamada, K., Bae, J. M., “Systhesis of Organic/Inorganic Nanocomposites Protonic Conducting Membrane Through Sol-Gel Processes”, *Solid State Ionics*,Vol. 118, pp. 29-36, March 1999.

Huang, R. Y. M, Pal, R., Moon,G. Y., *Journal of Membrane Science*, Vol. 160, pp. 101, 1999.

Jang, L. K., Nguyen, D., Geesey, G. G., *Water Res.*, Vol. 33, pp. 2826, 1999.

Jannasch, P., *Current Opinion in Colloid and Interface Science*, Vol. 8, pp. 96, 2003.

Jonissen, L., Gogel, V., Keres, J., Garche, J., *Journal of Power Sources*, Vol. 105, pp. 267 –73, 2002.

Karadedeli, B., Bozkurt, A., Baykal, A., *Physica*, Vol. B 364, pp. 279–284, 2005.

Kawahara, M., Rikukawa, M., Sanui, K., Ogata, N., *Solid State Ionics*, Vol. 136–137, pp. 1193 –6, 2000.

Kawahara, M., Rikukawa, M., Sanui, K., *Polymer Advanced Technology*, Vol. 11, pp. 544–7, 2000.

Kim, J. D., Honma, I., *Solid State Ionics*, Vol. 176, pp. 979-984, 2005.

Korgesch, K., Simader, G., *Fuel Cells and Their Applications*, Vol. 3 and 4, pp. 32, 1996.

Kotov, S. V., Pederesen, S. D., Qui, W. Z. M., Burton, D. J., *Jornal of Fluorine Chem.*, Vol. 82, pp. 13, 1997.

Kreuer, K. D.,Weppner, W., Rabenau, A., *Angew. Chem.*, Int. Ed., Vol. 21, pp. 208, England, 1982.

Kreuer, K. D., "Fast Proton Transport in Solids", *Journal of Molecular Structure*, Vol.177, pp 265-276, July 1988.

Kreuer K. D., Dipel, T. H.., Meyer, W. H., Maier, J., "Perfluorinated Ionemer Membranes", *Proceedings of the First International Symposium on Material Research Society*, 10-21 April, Vol. 293, pp. 273-282, Mainz, 1993.

Kreuer, K. D., *Chemistry Materials*, Vol. 8, pp.610–641, 1996.

Kreuer, K. D., *Proceedings of the sixth Asian Conference on Solid State Ionic: Science and Technology*, 29 November-4 December, pp. 263, New Delhi, 1998.

Kreuer, K. D., *Solid State Ionics*, Vol. 136–137, pp. 149–60, 2000.

Kreuer, K. D., *Journal of Membrane Science*, Vol. 185, pp. 29–39, 2001.

Kufacı, M., Bozkurt, A., Tülü, M., *Solid State Ionics*, Vol. 177, pp. 1003, 2006.

Laskar, A.L., Chandra, S., "Superionic Solids Electrolytes Recent Trends", *Academic Press*, Inc., 1989.

Lass`egues, L.C., Desbat, B., Trinquet, O., Cruege, F., Poisignon, C., *Solid State Ionics,* Vol. 35(1–2), pp. 17–25, 1989.

Li, S., Zhou, Z., Zhang, Y., Liu, M., *Chemistry of Materials*, Vol. 17, pp. 5884, 2005.

Lide DR, *Handbook of Chemistry and Physics*, Boca Raton: CRC Press, 1995.

Linford, R. G., *Electrochemical Science and Technology of Polymers*, Ch. 7, Elsevier Science Publishers LTD., 1990.

Liu, W., Ruth, K., Rusch, G., *Journal of New Material Electrochemical Systems*, Vol. 4, pp. 227, 2001.

Munson, R. A., *Journal of Physical Chemistry*, Vol. 68(11), pp. 3374–77, 1964.

Munson, R.A., Lazarus, M.E., *Journal of Physical Chemistry*, Vol. 71(10), pp. 3245–48, 1967.

Murthy, N. S., Minor, H., *Polymer*, Vol. 31, pp. 996-1002. 1990.

Münch, W., Kreuer, K. D., Silvestri, W., Maier, J., Seifert, G., *Solid State Ionics*, Vol. 145, pp. 437–443, 2001.

Ohno, H., and Yamazaki, H., "Preparation and Characteristics of All Solid- State Electrochromic Display with Cation–Conductive Polymer Electrolytes", *Solid State Ionics*, Vol. 59, pp. 217-222, 1993.

Pennarun, P. Y., Jannasch, P., *Solid State Ionics*, Vol. 176, pp. 1849, 2005.

Poppe, D., Frey, H., Kreuer, K. D., Heinzel, A., Mu¨lhaupt, R., *Macromolecules*, Vol. 35, pp. 7936–41, 2002.

Pourcelly, G., Oikonomou, A., Hurwitz, H. D., Gavach, C., *Journal of Electroanalytical Chemistry*, Vol. 287, pp. 43-59, 1990.

Przyluski, J., Wieczorek, W., *Synthetic Metals*, Vol. 45, pp. 323-333, 1991.

Pu, H., Meyer, W. H, Wegner, G., *Journal of Polymer science: Polymer Physics,* Vol. 40(7), pp. 663–69, 2002.

Qingfeng, L., Hjuler H. A., Bjerrum, N. J., "Phosphoric acid doped polybenzimidazole membranes: Physicochenmical characterization and fuel cell applications", *Journal of Applied Electrochemistry,* Vol. 31, pp. 773–9, 2001.

Ratner, Maccllum, J.R., and. Vincent, C.A. (editors), Polymer Electrolyte Reviews, Ch. 7, *Applied Science Publihers L.T.D.*, 1987.

Rauhut, G., *Phys. Chem. Chem. Phys*., Vol. 5 and 7, pp. 91, 2003.

Reisinger, T. J. G., *Abhängigkeit der Leitfähigkeit Glasartiger Ionene von Druck und Temperatur*, Ph. D. Thesis, Johannes Gutenberg Universitt, 1998.

Rieke, P. C., Vanderborgh, N. E., *Journal of Membrane Science*, Vol. 32, pp. 313-328, 1987.

Rietz,. R. R., Meyer,W. H., *Polymers for Advanced Technologies*, Vol. 4, pp. 164, 1993.

Rietz, R.R., Rohr, K. S., Meyer, W. H., Spiss, H. W., Wegner, G., *Solid State Ionics*, Vol. 68, pp.151-158, 1994.

Rodriguez, D., Jegat, C., Trinquet, O., Grondin, J., Lass`egues, J.C., *Solid State Ionics,* Vol. 61(1–3), pp. 193–202, 1993.

Samms, S. R., Wasmus, S., Savinell, R. F., *Journal of Electrochemical Society*, Vol. 143, pp.1498, 1996.

Sartori, C., Finch, D. S., Ralph, B., Gilding, K., *Polymer*, Vol. 38, pp. 43, 1997.

Savadogo, O., Varela, F. J. R., *Journal of New Material Electrochemical Systems*, Vol. 4(2), pp. 93–97, 2001.

Savett, S. C., Atkins, J. R., Sides, C. R., Harris, J. L., Thomas, B. H., Creager, S. E., Pennington, W.T., DesMarteau, D. D., *Journal of Electrochemical Society*, Vol. 149, pp. A1527, 2002.

Schoolman, D., Trinquet, O., Lass`egues, J.C., *Electrochimica Acta,* Vol. 37(9), pp. 1619–21, 1992.

Schuster P., Zundel G., Sandorfy C. (editors), *The Hydrogen Bond*, North-Holland, Amsterdam, 1976.

Schuster, M., Meyer, W. H., Wegner, G., *Solid State Ionics*, Vol. 145, pp. 85–92, 2001.

Schuster, M. F. H., Meyer, W. H., *Annual Review of Materials Research*, Vol. 33, pp. 233-261, 2003.

Sevil, F., Bozkurt, A., *Journal of Physics and Chemistry of Solids*, Vol. 65(10), pp. 1659, 2004.

Sevil, F., Bozkurt, A., *Turkish Journal of Chemistry*, Vol. 29, pp. 117, 2005.

Singleton, R. W., Noether, H. D., Tracy, J. F., *Journal of Polymer Science: Polymer Symposium*, Vol. 19, pp. 65–76, 1967.

Smitha, B., Sridhar, S., Khan, A. A., *Journal of Membrane Science*, Vol. 259, pp. 10, 2005.

Steck, A. E., Stone, C., *in Proceedings of the 2nd International Symposium on New Materials for Fuel Cell and Modern Battery Systems*, pp. 792, O. Savagodo, P. R. Roberge, and T. N. Veziroglu, Editors, Montreal, Quebec, Canada, July 6-10, 1997.

Sumner, J. J., Creager, S. E., Ma, J. J. A., DesMarteau, D. D., *Journal of Electrochemical Society*, Vol. 145, pp.107, 1998.

Sun, R. J., Jordan, L., Forsyth, M., MacFarlane, D., *Electrochimica Acta*, Vol. 46, pp. 1703, 2001.

Takahashi, T., "High Conductivity Solid Ionic Conductors", *World Scientific Publications Co. Ptc. Ltd.*, 1989.

Tanaka, R., Yamamoto, H., Kawamura, S., Iwase, T., *Electrochimica Acta* ,Vol. 40(13) , pp. 2421–29, 1995.

Tanaka, R., Yamamoto, H., Shono, A., Kubo, K., Sakurai, M., *Electrochimica Acta* Vol. 45 (8–9) , pp. 1385–89, 2000.

Tang, H., Pintauro, P. N., *Journal of Applied Polymer Science*, Vol. 79, pp. 49–59, 2001.

Tillement, O., "Solid State Ionics Electrochemical Devices", *Solid State Ionics*, Vol. 68, pp. 9-33,1994

Voet, D., and Voet, J. G., *Biochemistry*, John Willey &Sons, New York,1992.

Wainright, J. S., Wang, J. T., Weng, D., Savinell, R. F., Litt, M., *Journal of Electrochemical Society*, Vol. 142(7), pp. L121–23, 1995.

Wang, F., Hickner, M., Kim, Y. S., Zawodzinski, T. A., McGrath, J. E., *Journal of Membrane Science*, Vol. 197, pp. 231–42, 2002.

Wasmus, S., Daunch, A., Moaddel, H., Rinaldi, P. L., Litt, M., Presented at 187 th *Electrochem. Soc.* Meet, Reno, Abstr. 466, 1995.

Wundelich, B., "Thermal Analysis", Ch.7, *Academic pres, Inc*., 1990.

Xing, B. and Savadogo, O., "Proton Conduction in Basic Doped Polybenzimidazole", *Proceddings of the Third International Symposium on New Materials for Electrochemical Systems*, pp. 261, Canada, 2005.

Yamada, M., Honma, I., *Electrochimica Acta*, Vol. 48, pp. 2411, 2003.

Yamada, M., Honma, I., *Journal of Physical Chemistry*, Vol. 108, pp. 5522, 2004.

Yamada, M., Honma, I., *Chem Phys. Chem.*, Vol. 5, pp. 724, 2004.

Yamada, M., Honma, I., *Polymer* , Vol. 45, pp. 8349-8354, 2004.

Yamada, M., Honma, I., *Angew Chem*, Int Ed., Vol. 43, pp. 3688, 2004.

Yamada, M., Honma, I., *Electrochimica Acta*, Vol. 50, pp. 2837–2841, 2005.

Yamada, M., Honma, I., *Polymer*, Vol. 46, pp.2986, 2005.

Yeo, R. S., McBreen, J. C., *Journal of Electrochemical Society*, Vol. 130, pp.533, 1983.

Zhou, Z., Li, S., Zhang, Y., Liu, M., Li,W., *Journal of American Chemical Society*, Vol. 127, pp. 10824, 2005.